Marine and Petroleum Geology 55 (2014) 214–229

Contents lists available at ScienceDirect

Marine and Petroleum Geology

journal homepage: www.elsevier.com/locate/marpetgeo

Evolution of pore-fluid pressure during folding and basin contraction in overpressured reservoirs: Insights from the Madison–Phosphoria carbonate formations in the Bighorn Basin (Wyoming, USA)

Nicolas Beaudoin [a,b,*], Olivier Lacombe [a,b], Nicolas Bellahsen [a,b], Khalid Amrouch [c], Jean-Marc Daniel [d]

[a] UPMC Univ Paris 06, UMR 7193, ISTEP, F-75005 Paris, France
[b] CNRS, UMR 7193, F-75005 Paris, France
[c] Australian School of Petroleum, Centre for Tectonics, Resources and Exploration (TRaX), University of Adelaide, North Terrace, Adelaide, SA 5005, Australia
[d] Geology Geochemistry Geophysics Direction, IFP Energies Nouvelles, Rueil-Malmaison, France

ARTICLE INFO

Article history:
Received 25 July 2013
Received in revised form
26 November 2013
Accepted 12 December 2013
Available online 21 December 2013

Keywords:
Fluid pressure
Overpressure reservoir
Stress tensor
Fracture population
Basin contraction
Fold development

ABSTRACT

Reconstructing the evolution of paleofluid (over)pressure in sedimentary basins during deformation is a challenging problem, especially when no hydrocarbon-bearing fluid inclusions are available to provide barometric constraints on the fluid system. This contribution reports the application to a natural case (the Bighorn Basin) of recent methodological advance to access fluid (over)pressure level prevailing in strata during sub-seismic fracture development. The fluid pressure evolution in the Mississippian-Permian Madison–Phosphoria limestone reservoir is tentatively reconstructed from the early Sevier Layer Parallel Shortening to the Laramide folding in two basement-cored folds: the Sheep Mountain Anticline and the Rattlesnake Mountain Anticline. Results point out that supra-hydrostatic pressure values prevail in the limestone reservoir during most of its whole Sevier–Laramide history. The comparison of the reconstructed fluid overpressure values within situ measurements in various overpressure reservoirs in other oil-producing basins highlights that the supra-hydrostatic fluid pressure gradually reaches the lithostatic value during the whole basin contraction and fold development. During most of the LPS history, however, overpressure level can be defined by a mean gradient. Among the factors that control the pressure evolution, the mechanical stratigraphy, the stress regime under which fractures developed and regional fluid flow are likely dominating in the case of the Bighorn Basin, rather than classical factors like disequilibrium compaction or fluid generation during burial. A coeval evolution between fluid overpressure and differential stress build-up is also emphasized. The approach presented in this paper also provides estimates of strata exhumation during folding.

1. Introduction

Many oil producing basins currently experience abnormally pressured fluid reservoirs governed by supra-hydrostatic fluid pressure, (*i.e.* fluid overpressure, e.g. Hunt, 1990). The importance and evolution of such fluid overpressure (*i.e.*, above the hydrostatic fluid pressure) are key but debated questions in Earth sciences, since the fluid pressure is associated to seismic cycle in various P-T conditions (Sibson, 1989; Zoback and Townend, 2001; Raimbourg and Kimura, 2008; Sibson, 2012), hydrofracturing (Cornet et al., 2003a; Bons and Elburg, 2012), gravitational sliding of rocks (Mourgues and Cobbold, 2006), evolution of fluid system through time (e.g. Evans and Fischer, 2012), and (re)activation of faults (Cornet and Morin, 1997; Cobbold et al., 2001; Cornet et al., 2003b; Douglas et al., 2003; Mourgues and Cobbold, 2003; Cobbold et al., 2004; Cornet et al., 2007; Lacroix et al., 2013; Leclère et al., 2013; Sibson, 2013; Moore et al., 2013). Fluid (over)pressure is also an important factor controlling economic fluid generation and migration, such as hydrocarbons or ore-forming hydrothermal fluids. In addition, fluid pressure is a governing factor of the evolution of permeability and porosity of limestones (Van Geet et al., 2002; Roure et al., 2005, 2010), and therefore a key parameter in reservoir studies and for basin modeling purposes. However, values from natural examples are still lacking in models to be fully interpreted (Bour and Lerche,

* Corresponding author. Current address: School of Geographical and Earth Sciences, University of Glasgow, Gregory Building, G128QQ Glasgow, United Kingdom.
E-mail addresses: Nicolas.beaudoin@glasgow.ac.uk, nebeaudoin@gmail.com (N. Beaudoin).

0264-8172/$ – see front matter © 2013 Elsevier Ltd. All rights reserved.
http://dx.doi.org/10.1016/j.marpetgeo.2013.12.009

1994; Yu and Lerche, 1996; Nysæther, 2006). Consequently, estimating fluid pressure in rock reservoirs is a first-order target for both industrial and academic purposes.

While fluid temperature can easily be determined in active and fossil systems thanks to fluid inclusions and stable isotopes, reconstructing the fluid pressure evolution requires either direct measurements in boreholes in active systems or analysis of hydrocarbon-bearing fluid inclusions from mineralized fault rocks and veins in fossil systems (e.g. Pironon and Bourdet, 2008; Becker et al., 2010; Bourdet et al., 2012; Fall et al., 2012). Thus, few methods have been proposed so far to reconstruct the fluid pressure during deformation that affected sedimentary strata in basins (Philipp, 2012) where oil or gas-bearing inclusions are absent. Consequently, our understanding of the evolution of fluid pressure in folded strata during deformation remains scarce and mainly theoretical.

Amrouch et al. (2011) show that the question of fluid pressure evolution in carbonates can be addressed by using calcite twin paleopiezometry together with fracture analysis and rock mechanics. They used the approach proposed by Lacombe and Laurent (1992) to reconstruct the absolute stress tensor (both principal stress orientations and magnitudes) to quantify the fluid pressure during the development of fractures recognized in the Sheep Mountain Anticline (SMA), a Laramide basement-cored anticline in the Bighorn Basin (BHB), Wyoming, USA.

Using this approach, this contribution aims at constraining the evolution of fluid overpressure and to discuss the controlling factors during the Sevier and Laramide Layer-Parallel Shortening (LPS) phases and subsequent Laramide folding at the scale of the BHB, and at estimating syn-folding exhumation of strata. We rely on the papers by Amrouch et al. (2011) and Beaudoin et al. (2012) which report in detail the sequence of fracture development and the associated paleostress evolution in thrust-related folds on both sides of the BHB, the SMA and Rattlesnake Mountain Anticline (RMA), and therefore provide accurate microstructural and relative time frames for the study. We focus on the Mississippian-Permian limestones of the Madison and Phosphoria formations that crop out on both sides of the basin and which are of primary importance for hydrocarbon exploration (Fox and Dolton, 1996). The reconstructed fluid pressure evolution is compared to the fluid flow history of the BHB (Beaudoin et al., 2014). This comprehensive approach provides the opportunity to discuss the parameters that control fluid pressure in a continuous limestone reservoir during basin contraction. In addition to classical factors causing fluid overpressure such as chemical compaction (including disequilibrium compaction and fluid production mechanisms, e.g. Yassir and Bell, 1996; Cobbold et al., 2013), or porosity variation/deformation due to stress build-up (e.g. Roure et al., 2010), the impact of large-scale fluid migration is also tested, both regarding the lateral transfer in the reservoir at the basin-scale and the fold-scale vertical migration of exotic fluids when no compartmentalization prevails in strata. Finally, the reconstructed overpressure values are compared to measurements of fluid pressure in overpressure reservoirs from other oil-producer basins worldwide and to reconstructions of paleofluid pressure evolution during fracture opening, based on oil-bearing fluid inclusions. This comparison highlights the role of lithology and the impact of both the stress regime and the structural evolution on the fluid overpressure in deforming sedimentary reservoirs.

2. Geological setting & dataset

2.1. Structural setting

The Bighorn Basin is an intracratonic basin developed in the frontal part of the Sevier-Laramide Rocky Mountains, from late Jurassic to Paleocene (DeCelles, 2004; Fig. 1 a). During the Sevier thin-skinned contraction, the current BHB was located in the foreland of the current Idaho-Wyoming range, the Western Interior Basin, from which far-field stresses were transmitted forelandward, leading to the development of diffuse fracture sets in the different parts of the basin (Varga, 1993; Craddock and Van der Pluijm, 1999; Neely and Erslev, 2009; Amrouch et al., 2010a; Beaudoin et al., 2012; Weil and Yonkee, 2012). During the Laramide thick-skinned contraction, part of the Western interior basin was incorporated into the fold-thrust belt, with the reactivation of basement thrusts causing basement-cored folding on its edges while Paleocene and Eocene rock were still depositing in the central part, forming the current BHB (Fig. 1 b, c). The largest of these thick-skinned structures are the so-called Laramide Arches that isolated the basin on the East, West and South early during the Laramide contraction. Among the folds of the BHB, we focused on two folds that were intensively studied on a structural point of view, along with the characterization of the sequence of fractures and the reconstruction of paleostress/strain history: the Sheep Mountain Anticline (SMA), located on the eastern part of the BHB, and the Rattlesnake Mountain Anticline (RMA) on the western part of the BHB.

The SMA is an NW–SE striking, 20 km long and 5 km wide, basement-cored asymmetrical anticline (Stanton and Erslev, 2004). Its backlimb is dipping 30°SW and its forelimb is dipping 70°NE (Fig. 1 d). The SMA exhibits well-preserved sedimentary rocks from the upper part of the Mississippian limestones/dolostones of the Madison formation to the Permian limestones of the Phosphoria formation, overlain by the gypsum of the Triassic Gypsum Spring formation (Fig. 1 b). The RMA is an NW–SE striking, 27 km long and 12 km wide, basement-cored and asymmetrical anticline, archetypal of draped folds (Stearns, 1971; Erslev, 1995). Its backlimb is gently dipping 50°NE while its forelimb is dipping 50°SW (Fig. 1 d). Above the Precambrian granitic basement that is exposed in the southern part of the fold, the whole Paleozoic sedimentary succession crops out at RMA, including the Cambrian sandstones of the Flathead and the Gallatin formations separated by the Gros Ventre shaly formation. Those formations are overlain by the Ordovician dolostones of the Bighorn Formation, the Devonian sandstones of the Three Forks formation, the Mississippian limestones/dolostones of the Madison Formation, the Mississippian shales and sandstones of the Amsden Formation, the Pennsylvanian sandstones of the Tensleep Formations, and the Permian limestones of the Phosphoria Formation (Fig. 1 b).

2.2. Microstructural setting

The SMA and RMA exhibit fracture populations that have been deciphered and interpreted in previously published works (summarized on Fig. 2; Harris et al., 1960; Johnson et al., 1965; Bellahsen et al., 2006a,b; Neely and Erslev, 2009; Amrouch et al., 2010a; Savage et al., 2010; Beaudoin et al., 2012). During the Laramide compressional history of the basin, brittle deformation was nearly homogeneously distributed throughout the basin, while most of Sevier-related fracture sets can only be observed in its western part. The following is a summary of the fracture sequence proposed by Beaudoin et al. (2012, Fig. 2).

The first fracture set related to the Sevier contraction consists of bed-perpendicular joints/veins striking E-W once corrected for strata tilting, developed in a strike-slip stress regime in response to the far-field orogenic stress (set S-I). This set S-I developed as a systematic fracture set only at RMA. Set S-II consists of a set of bed-perpendicular, joints/veins oriented N–S once corrected for strata tilting and developed in an E-W extensional stress regime and observed mainly in the western part of the basin and postdating set S-I. This set S-II has been tentatively related to the late Cretaceous

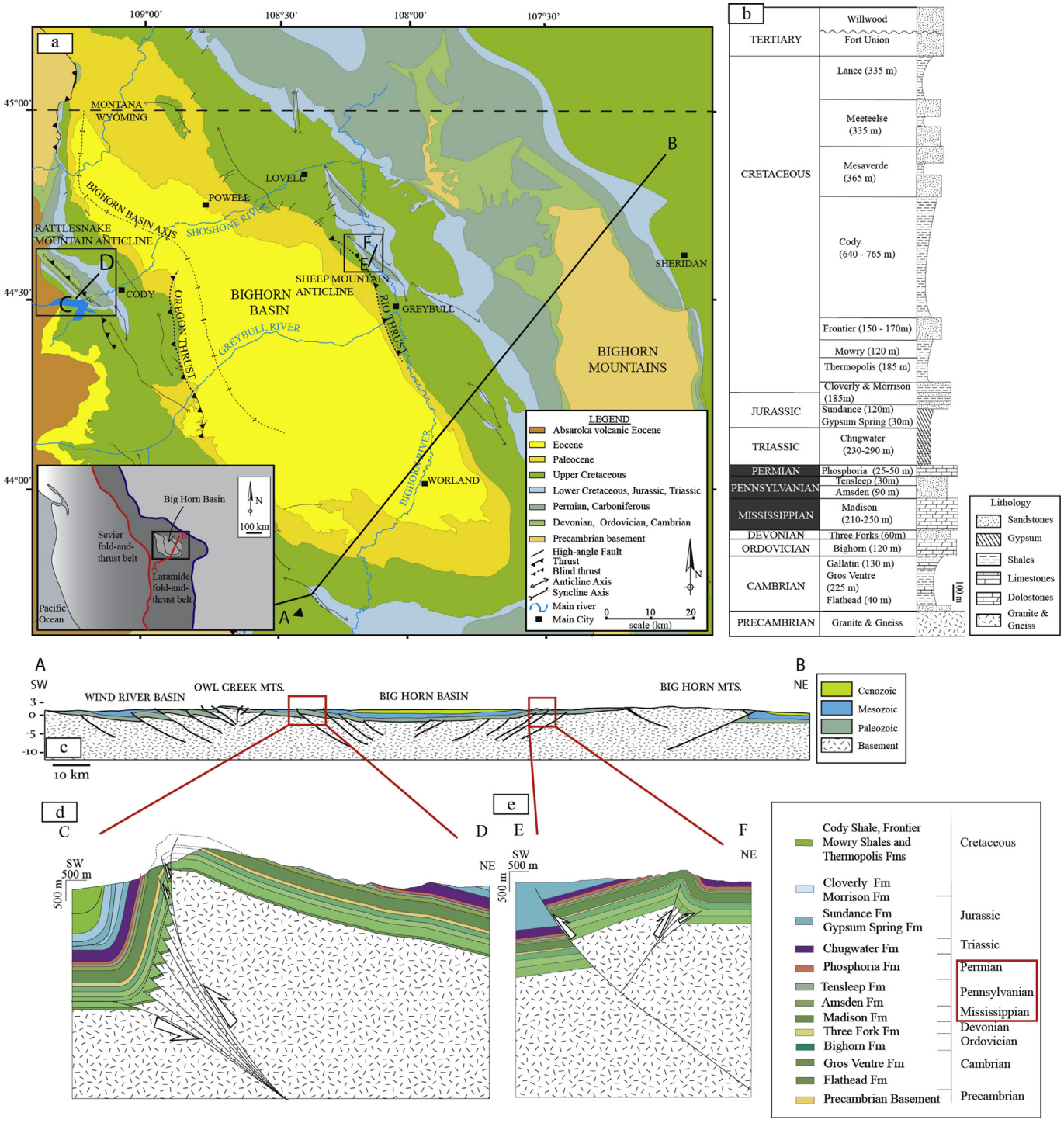

Figure 1. a – simplified geological map of the Bighorn Basin (modified after Beaudoin et al., 2014), with location of the studied anticlines Rattlesnake Mountain (RMA) and Sheep Mountain (SMA). Lines A-B, C-D and E–F locate cross-sections of Figure 1 c, d and e, respectively. Insert represents the Western part of the USA in the current geographic position; red line represents current morphological front of the Sevier thrust-belt and blue line Laramide thrust-belt. b – Stratigraphic column of the Bighorn Basin (Durdella, 2001). The limestone reservoir studied is highlighted with gray underlining. c – NE–SW cross-section of the Laramide Belt based on seismic data (modified after Love and Christiansen, 1985; Stone, 1987). Red frames are location of lateral equivalents of RMA and SMA. d, e – SW–NE cross-section of RMA (d) and SMA (e) after Beaudoin et al. (2012). Red frame in the legend is relative to the Madison–Phosphoria reservoir. (For interpretation of the references to color in this figure legend, the reader is referred to the web version of this article.)

foreland flexural evolution of the basin. Tectonic stylolites reflect a 110°–135°E contraction which is also associated with third Sevier-related fracture set at basin-scale (set S-III), consisting of bed-perpendicular joints/veins striking 110°E once corrected for strata tilting related to a WNW-ESE strike-slip stress regime. In spite of being observable at both SMA and RMA, these fractures appear stratabound at SMA while they display a higher vertical persistence at RMA (Barbier et al., 2012a; b). The last Sevier-related fracture set consists of reverse faults at RMA and strike-slip faults at SMA, related to late Sevier LPS phase (set S-LPS4).

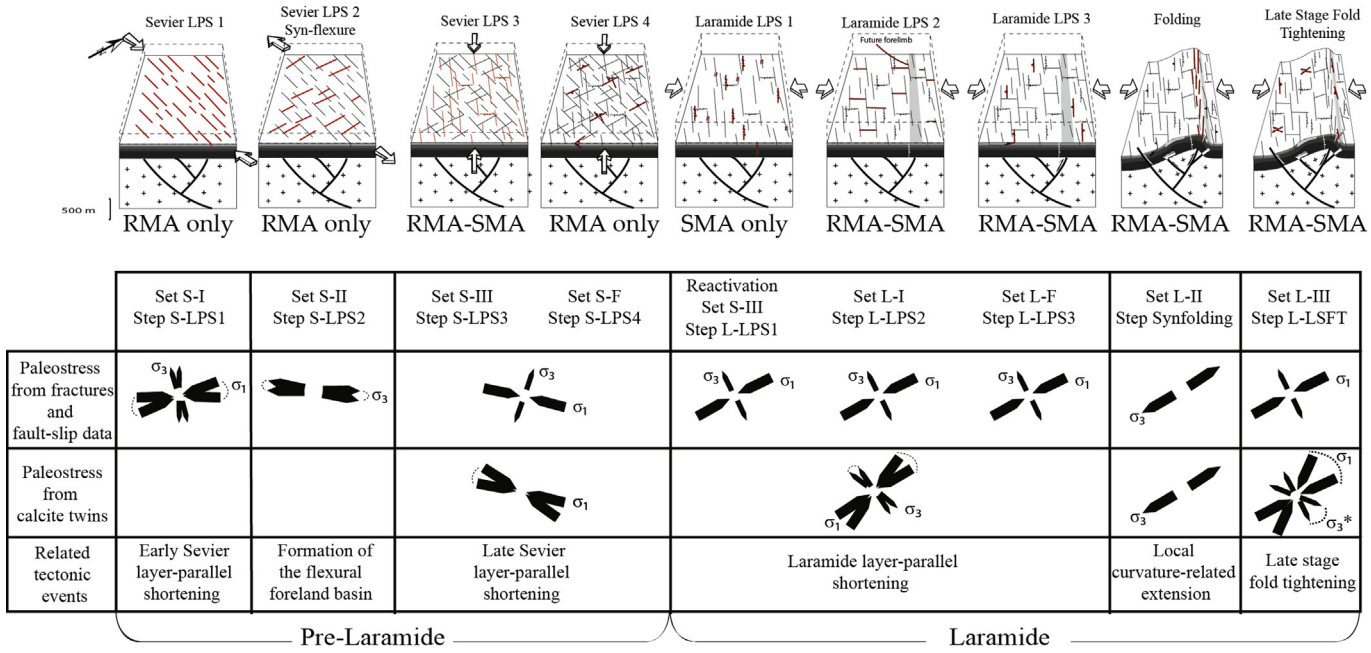

Figure 2. Kinematic, microstructural and paleostress evolutions of RMA and SMA during Sevier and Laramide tectonics. Paleostress evolution is derived from the study of calcite twins, fractures and striated microfaults from Amrouch et al. (2010a) and Beaudoin et al. (2012).

The Laramide LPS was first marked by the left-lateral reactivation of set S-III veins documented at SMA (LPS L-0), followed by the development of tectonic stylolites and of a set of 045°E-oriented, bed-perpendicular veins/joints at basin-scale (set L-I) reflecting a strike-slip stress regime. A late feature related to Laramide LPS is a set of reverse faults observed at both RMA and SMA (set L-LPS3). The folding step is associated with a set of bed-perpendicular joints/veins striking 135°E (set L-II), formed in a local extensional stress regime due to strata bending at fold hinge. During the late stage fold tightening, a third Laramide-related fracture set developed as small-scale strike-slip and reverse conjugate faults, while well-oriented preexisting joints/veins formed during previous stages were reactivated in the forelimb of both folds (set LSFT).

Twinned calcite from veins and host rocks was previously studied using the Calcite Stress Inversion technique (Etchecopar, 1984; for a summary see Lacombe, 2010) in order to determine paleostress orientations and differential stress magnitudes (Amrouch et al., 2010a; Beaudoin et al., 2012). This method allows simultaneous computation of principal stress orientations and differential stress magnitudes for each twinning event. Relative timing of the stress tensors reconstructed this way was established by considering the orientation of principal stress orientations with respect to strata dip (hence for identifying pre/early-, syn- and late/post folding stress regimes) and/or vein orientation within the fracture sequence. In the present study, we use the results of calcite twinning paleopiezometry reported by Amrouch et al. (2010a) and Beaudoin et al. (2012) for SMA and RMA, respectively.

3. Methodology

3.1. Basic principles

In order to quantify fluid pressure, we have first applied the method proposed by Lacombe and Laurent (1992). The method consists of finding for each deformation step, using a simple Mohr construction, the effective values of σ_1, σ_2 and σ_3 required for consistency between differential stresses estimated from calcite twinning, frictional sliding along preexisting planes (i.e., Byerlee's law) and newly formed faulting/fracturing (Fig. 3). We rely on available rock mechanics tests previously performed on fresh samples of the Madison and Phosphoria formations from SMA (Amrouch et al., 2011). The intrinsic failure envelope used to account for newly formed fracturing/faulting in our Mohr diagrams reconstruction is the mean crack–development curve (dilatancy) for both formations, because we believe that it better represents the in situ mechanic properties of an heterogeneous natural material than the failure curve (Mohr–Coulomb) determined from intact rock samples (e.g. Lacombe, 2001).

To access fluid pressure prevailing in the strata at each step of the deformation, we first assume that one principal stress is generally vertical or close to vertical (Lacombe, 2007) and therefore equal to the effective weight of overburden. We therefore calculate the difference between the theoretical effective vertical principal stress σ_{vth} and the effective vertical principal stress σ_{veff} inferred from our Mohr constructions to define $\Delta\sigma_v$ (Fig. 3). σ_{vth} is calculated as the difference between lithostatic and hydrostatic pressures ($\sigma_{vth}=(\rho_{rock} - \rho_{water})^*g^*h$). A non-zero $\Delta\sigma_v$ can therefore be explained either by fluid over- or under-pressure or by burial changes (sedimentation or erosion). $\Delta\sigma_v$ was calculated at each step of the deformation, (Fig. 3). When $\Delta\sigma_v$ is positive, either the burial depth was less than the value considered for the calculation of σ_{vth}, or the system was overpressured (Figs. 5 and 6).

3.2. Application to SMA and RMA

In order to calculate $\Delta\sigma_v$ for both SMA and RMA for all substages of the microstructural evolution, we considered the sources of changes in the σ_{vth} value. In terms of changes of the burial depth of the investigated Madison–Phosphoria formations over the Sevier and Laramide contractional events, one has to take into account deposition of the upper Cretaceous Cody Shales Formation in between (Fig. 4 a, DeCelles, 2004). This consideration allows the determination of the thickness of overburden with respect to log

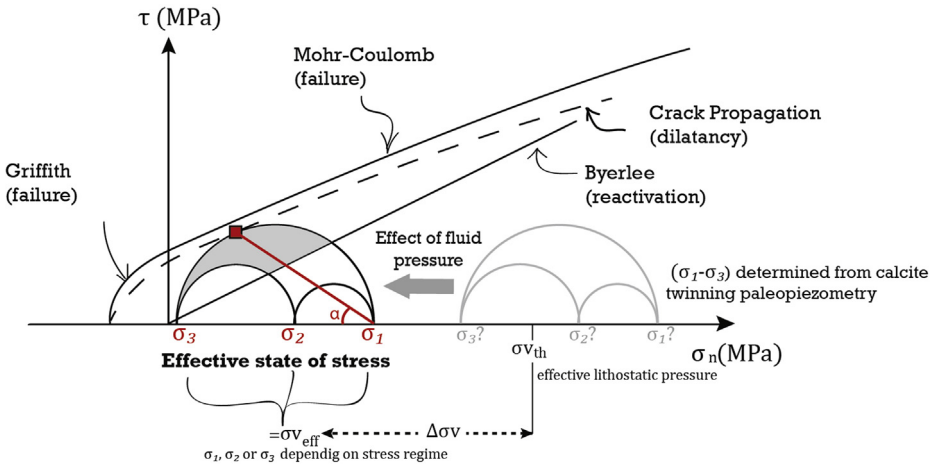

Figure 3. Schematic representation of the method proposed by Lacombe and Laurent (1992) to access the absolute stress tensor from calcite twinning paleopiezometry, along with graphical definition of $\Delta\sigma_v$, σ_{vref} and σ_{veff} used after the method proposed by Amrouch et al. (2011) to assess fluid overpressure evolution.

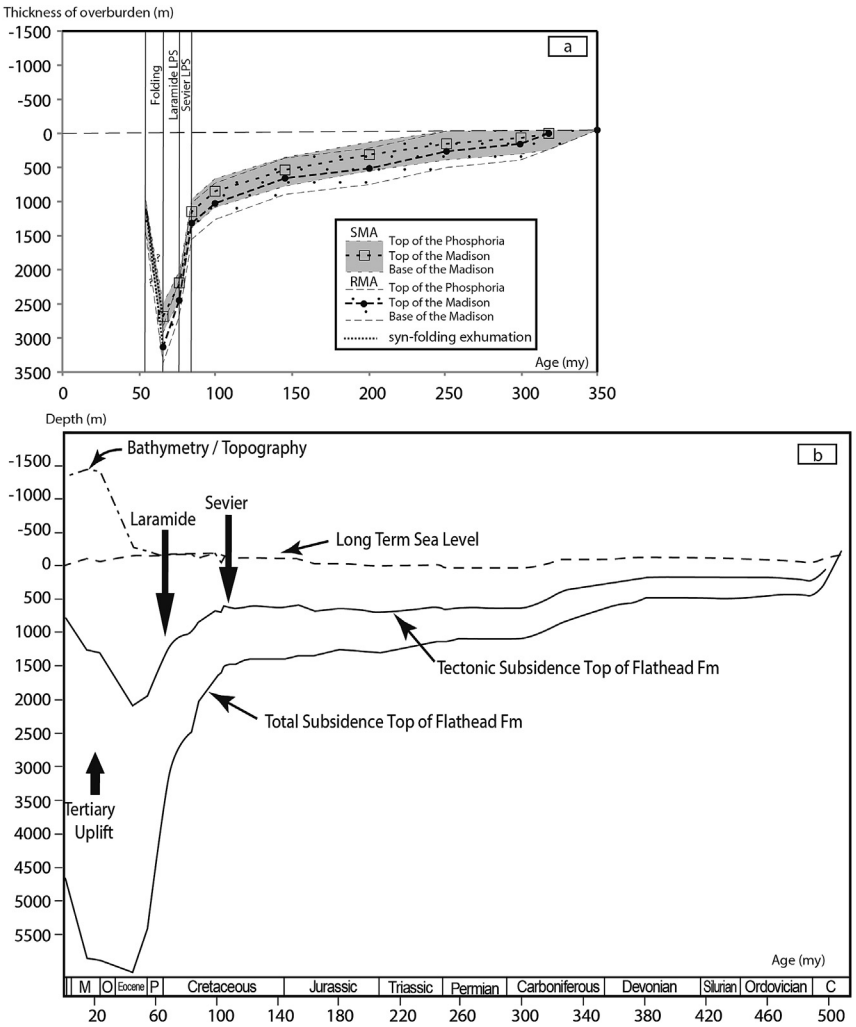

Figure 4. A. Burial curves reconstructed for the limestone reservoir Madison–Phosphoria for the RMA and the SMA. Thick dotted lines represent the top of the Madison Formation for the SMA and the RMA, while thin dotted lines the base of the Madison Formation and the top of the Phosphoria Formation. These curves show the thickness of overburden along time, and take into account the syn-folding exhumation reconstructed in this study (see text for details, Pierce, 1966; Pierce and Nelson, 1968; Hennier, 1984; Rioux, 1994). B. Subsidence history of the basin, based on well data at 25 km eastward away from Cody, Wy (so ~30 km eastward away from the RMA). This subsidence history concerns the top of the Cambrian Flathead Fm, i.e. ~700 m below the base of the Madison Fm (modified after May et al., 2013).

data, during the Sevier (from the top of the Phosphoria Fm to the bottom of the Cody Shales Fm) and during the Laramide (from the top of the Phosphoria Fm to the top of the Cody Shales Fm). The burial depth evolution has been reconstructed for the base and top of the Madison Fm and for the top of the Phosphoria Fm (Fig. 4 a) based on stratigraphic sections reconstructed in synclines (Pierce, 1966; Pierce and Nelson, 1968; Hennier, 1984; Rioux, 1994) and on recent U/Pb analysis on detrital zircons on the edges of the basin (May et al., 2013). The subsidence history of the top of the Cambrian Flathead Fm in the center of the basin is also presented for comparison (Fig. 4 b, modified after May et al., 2013). Consequently, a relative error about burial due to compaction must be considered but was not taken into account, as the compaction factors for the concerned strata remain unknown. Considering the location of SMA and RMA on the edge of the basin, and that almost no Tertiary sediments deposited after the Cody Shales (Hennier, 1984; Roberts et al., 2008), neglecting burial changes due to sedimentation during Laramide times is a viable assumption. Indeed, deposition of the upper Campanian-Maastrichtian sediments, which form the Mesaverde and Meeteetse Formations, started after 76 Ma (May et al., 2013), and this time is considered as the beginning of the Laramide tectonics (Dickinson et al., 1988; DeCelles, 2004). In addition, these formations are not present close to the folds, being observed in the interior of the BHB (Thomas, 1965). Thus, we assumed that neither burial nor exhumation occurred during Laramide LPS at the scale of SMA and RMA. The same assumption for the Sevier phase is less robust. However, we assume that most of the recorded deformation postdates the development of the Sevier Range forebulge (Beaudoin et al., 2012). This event occurred during Turonian times (DeCelles, 2004), which suggests that most of the Sevier related deformation affecting the basin occurred from the late Turonian until the Upper Campanian, corresponding to the deposition of the 1000m-thick Cody Fm (Finn et al., 2010; May et al., 2013).

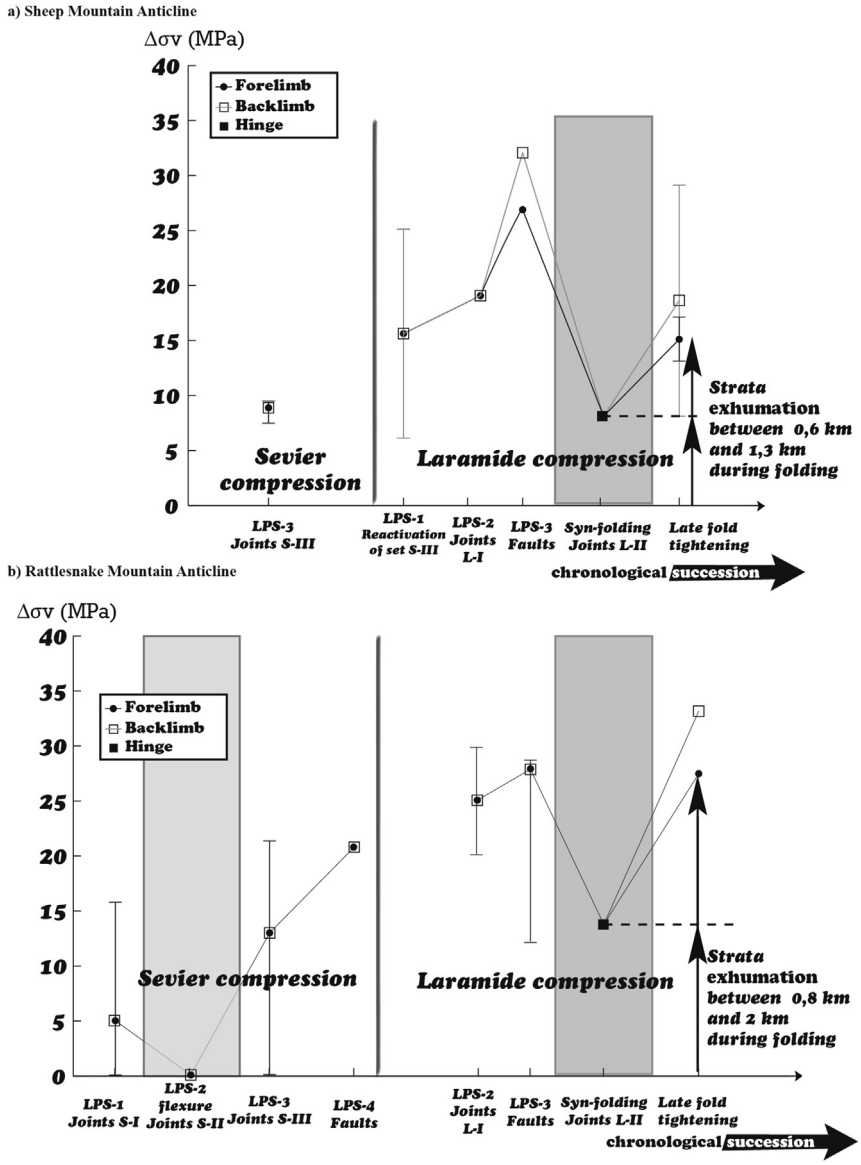

Figure 5. Evolution of the difference $\Delta\sigma_v$ between the theoretical effective vertical principal stress and the effective vertical principal stress reconstructed using the method illustrated in Figure 3. The difference in overburden from the Sevier to Laramide is 1 km for both SMA and RMA. Exhumation is reconstructed during late stage fold tightening considering two different hypotheses discussed in the text and represented by the dotted line. Reported error bars reflect uncertainties about the stress ellipsoid shape (ϕ) ratios obtained from stress inversion of calcite twin data and fault-slip data.

We also consider that folding occurred early during the Laramide history because of the early exhumation of Laramide arches (such as the Bighorn Mountains) at the very end of Cretaceous times as documented by Crowley et al. (2002). After folding, one can no longer consider that the overburden value can be deduced directly from log data because of the structural relief formation that led to partial, and likely rapid, erosion of the stratigraphic column considering the climatic conditions during the Paleocene (Koch et al., 1995). To further interpret the value of $\Delta\sigma_v$, it is therefore required to estimate either the overburden thickness or the fluid overpressure remaining in the reservoir (Fig. 5). Recent reconstructions of fluid system evolution in the Bighorn Basin based on the very same fracture system at the scale of SMA (Beaudoin et al., 2011) and RMA (Beaudoin et al., 2014) point out that the fold-related joint sets connected the whole stratigraphic column, triggering fast fluid migration inside and outside of the Madison–

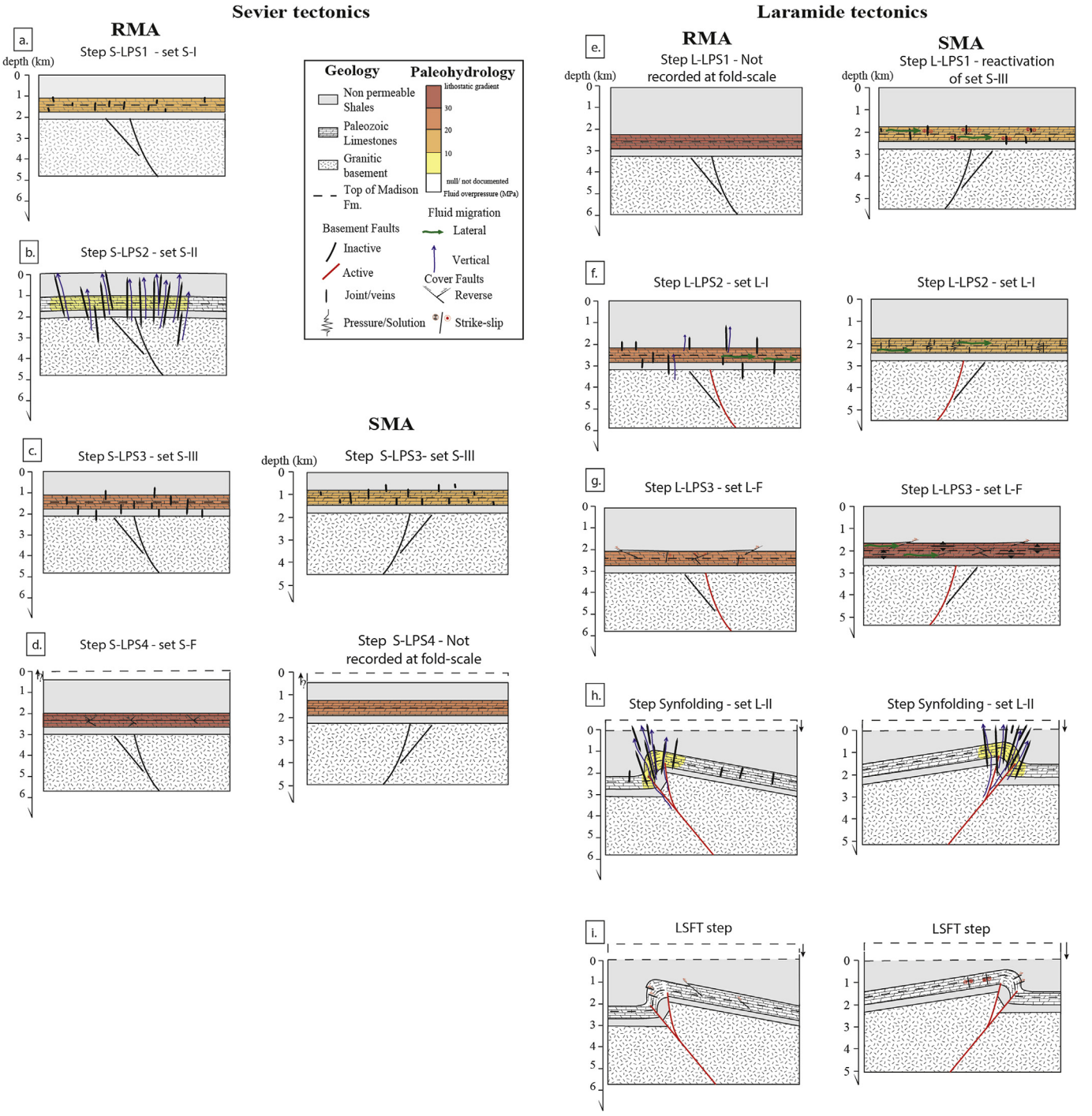

Figure 6. Evolution of burial, deformation, fluid migrations and fluid overpressure level in the Madison–Phosphoria reservoir at the scale of RMA and SMA during the Sevier (a–d) and Laramide (e–i) tectonics. The fluid overpressure is reported using yellow to red color scale according value of overpressure reconstructed regarding burial depth. Fluid migrations in and out the reservoir are reported according to Beaudoin et al. (2014). On sketchs, dotted lines in the reservoir mark the top of the Madison Fm, and correspond to the same stratigraphic level as the dotted lines in Figure 4 a. (For interpretation of the references to color in this figure legend, the reader is referred to the web version of this article.)

Phosphoria reservoir. This study supports the overall observation that syn-folding fractures caused a high vertical hydraulic permeability that connects strata (Sibson, 2004; Fischer et al., 2009; Evans and Fischer, 2012), and suggests an efficient exhaust of fluids out of the limestone strata and thus justifies the preliminary assumption that the fluid overpressure likely decreased to nearly 0 just after folding. From this time onward, and assuming zero fluid overpressure after folding, the value of $\Delta\sigma_v$ can therefore be interpreted as reflecting a variation of overburden thickness that correspond to burial in the case where $\Delta\sigma_v$ value becomes negative after folding and therefore to exhumation if $\Delta\sigma_v$ value remains positive.

The post-folding $\Delta\sigma_v$ value can be used to calculate the eroded/burial thickness E:

$$E = \Delta\sigma_v/((\rho_r - \rho_w)^*g) \quad (1)$$

as well as the post-folding overburden thickness h':

$$h' = (\sigma_{vth} - \Delta\sigma_v)/((\rho_r - \rho_w)^*g) \quad (2)$$

For the calculation of σ_{vth} we use an overburden thickness variation of 1.1 km in the West and 1 km in the East between Sevier and Laramide times, which corresponds to the thickness of the Cretaceous Cody shales (DeCelles, 2004; May et al., 2013). At RMA, the overburden is about 1.3 km during Sevier time and 2.4 km during Laramide time while at SMA, it is about 1.1 km during Sevier time and 2 km during Laramide time. The complete Mohr diagram constructions are available in Amrouch et al. (2011) and in Beaudoin et al. (2012) for SMA and RMA, respectively, and are consequently not reported in the present paper for the sake of simplicity. Stress magnitudes and $\Delta\sigma_v$ at each step are however summarized in Table A (supplementary material).

3.3. Up-scaling results from folds to basin-scale

To better understand how fluid overpressure may have evolved during deformation, we tentatively up-scaled the results obtained at fold-scale to the scale of the entire Bighorn Basin. To do so, we compared the $\Delta\sigma_v$ evolution at RMA and at SMA (Fig. 6). At this stage, the effect of increasing depth on differential stress magnitude (e.g., Lacombe, 2007) must be taken into account to reliably compare fluid overpressure magnitudes derived at different depths from values of $\Delta\sigma_v$. We thus normalized the differential stress magnitudes considering a common depth of burial of 2 km. So, every differential stress magnitude from RMA and from the Sevier compression at SMA was corrected according to the type of the stress regime following the equations of Jaeger and Cook (1969) used in Lacombe (2007). We considered a fluid pressure ratio of $\lambda = 0.7$ to reflect the supra-hydrostatic state that prevails in strata and a friction coefficient $\mu = 0.8$. Consequently, new representations of the state of stress on Mohr diagrams were done and new $\Delta\sigma_v$ were calculated for each deformation step when needed.

3.4. Uncertainties for the fluid overpressure and exhumation estimates

The uncertainties on the reconstruction of $\Delta\sigma_v$ and consequently E are due to various factors. First, the calcite twinning paleopiezometry estimates a peak differential stress with a relative error of about 20%. This uncertainty has been taken into account for the reconstruction of Mohr diagrams, and is reduced to a negligible uncertainty in most of case where Mohr circle size is limited by the crack development curve. This crack development curve, reconstructed from mechanical tests on limestones from outcrops of Madison and Phosphoria Fms at SMA, is used as an approximation of the Mohr–Coulomb criterion for a heterogeneous material deformed at depth. The use of this crack development curve also implies a relative error, but as most of the deformation occurred after compaction of strata, it can be considered as witnessing the mechanical condition of strata at depth. A third source of uncertainty is related to the value of the stress ellipsoid shape ratio (Table A column ϕ, provided as supplementary material) when the stress regime was strike-slip in nature. This affects the value of σ_{veff} in a dramatic way, and this is the largest source of error on this method, which explains most of the error bars that are reported on Figure 5. Another source of uncertainty is the burial depth evolution. As discussed earlier, this cannot be precisely constrained mainly because compaction factors and independent estimates based on fission tracks in apatite are not available in the literature. However, for an error of about 300 m (10% of the maximum burial), the change on σ_{vth} is about 4–5 MPa, which remains small compared to the increase of $\Delta\sigma_v$ of about 20 MPa during LPS phases (Fig. 5). At last, the possibility that one principal stress could have been not always vertical can change the estimated value of σ_{veff}. Amrouch et al. (2011) calculated that for an average 20° dip of the backlimb, considering a stress rotation during folding, hence a bed-perpendicular principal stress axis instead of a vertical one, would lead to a misestimate of only 4 MPa for $\Delta\sigma_v$. Nevertheless, as most of the stress tensors where reconstructed in fractures perpendicular to strata, this correction would have only concerned faulting events that occurred during strata tilting (set L-LPS3).

To sum up, it is clear that our reconstruction of fluid overpressure provides orders of magnitude rather than accurate values. Nevertheless, the consistency of the fold-scale evolution of $\Delta\sigma_v$ at large-scale and how it can be related to the evolution of fluid system reconstructed independently validate a posteriori these estimates and their evolving trends.

4. Results & discussion

4.1. Evolution of fluid pressure with Madison–Phosphoria limestone reservoir at the fold scale

Figure 5 shows the evolution of $\Delta\sigma_v$ in the Madison–Phosphoria reservoir at fold-scale, for SMA (Fig. 5 a) and for RMA (Fig. 5 b). In both cases, $\Delta\sigma_v$ values are not corrected from depth variation between Sevier and Laramide times, so the fluid overpressure evolution of the two tectonic events cannot be quantitatively compared. In the case of SMA, a fluid overpressure level about 8 MPa prevailed in strata during the Sevier compression and about 15 MPa since the beginning of the Laramide compression. A progressive increase in fluid overpressure is recorded during the whole LPS stage until the fluid overpressure level reaches a magnitude of 26 MPa in the forelimb and 33 MPa in the backlimb (Fig. 5 a). The classical but debated effect of disequilibrium compaction, which is commonly invoked as the main source of fluid overpressure in sedimentary basin (Yassir and Bell, 1996; Nordgard Bolas et al., 2004; Van Ruth et al., 2004) cannot easily be invoked in the present case. Indeed, beyond the fact that this mechanism applies well to very low permeability sedimentary rocks as shales, it requires a sedimentation rate larger than the rate of pore fluid expulsion. Yet, the location of RMA and SMA at the edges of the basin precludes considering significant sedimentary deposition during LPS phase, so that the disequilibrium compaction can be precluded from our reasoning as a governing mechanism for pore pressure evolution. Alternatively, this pore pressure increase in limestones may reflect (Fig. 6): (1) an effective reduction of porosity volume by pressure-solution (Amrouch et al., 2011); (2) a poor hydraulic permeability of the fracture set L-I, (as suggested from geochemical studies by Beaudoin et al., 2011) due either to mechanical stratigraphy

(Barbier et al., 2012a) or to a fast healing of cracks that do not allow fluids to escape from the limestone reservoir; (3) a strong increase in horizontal stress magnitude, which will impact pore fluid overpressure (Yassir and Bell, 1996); or (4) an input of exotic fluids into the reservoir in response to a large-scale fluid migration (as proposed in Beaudoin et al., 2014) which could cause fluid pressure increase, as documented in Cook Inlet Basin (Alaska, Bruhn et al., 2000). The difference in differential stress magnitudes, hence of $\Delta\sigma_v$ values between both limbs of the fold has already been related to the stress perturbation due to loading of, and onset of slip along, the underlying basement fault that caused asymmetrical distribution of fracture sets and of internal rock strain in fold limbs (Fig. 6 f; Bellahsen et al., 2006b; Amrouch et al., 2010a,b). The level of fluid overpressure at this step of deformation corresponds to a fluid pressure that reaches and could overcome the lithostatic pressure, which is supported by the development of bed-parallel veins observed on the field (Fig. 6 g, Amrouch et al., 2010a, 2011). The development of such bed-parallel veins (cone-in-cone or beefs) is a common feature in sedimentary basins (Cobbold et al., 2013; Smith et al., 2013) and can be related either to a not horizontal bedding in purely lithostatic condition or to a tensile vertical stress due to fluid overpressure, the latter being the most likely in our case. The evolution depicted in Figure 5 a has been implemented compared to Amrouch et al. (2011) by also considering the syn-folding value of $\Delta\sigma_v$ deduced from the requirement for tangency of the Mohr circle with the crack development curve to account for the formation of set L-II veins/joints in a local extensional regime due to strata bending at fold hinge. The resulting value is about 8 MPa, which is also the minimum overpressure value that prevailed in the reservoir during the whole deformation history recorded in the SMA. It is difficult to interpret this $\Delta\sigma_v$ value directly in terms of fluid overpressure, because folding caused topography and so erosion and exhumation (Fig. 6 h–i). Thus, we can consider that the syn-folding $\Delta\sigma_v$ corresponds to the maximum fluid overpressure remaining in the strata, because if this value also includes an efficient syn-folding exhumation, the fluid overpressure reconstructed will be below the one suggested by $\Delta\sigma_v$ value. In any case, development of curvature-related fracture set trigger a strong decrease in fluid overpressure, suggesting that set L-II joints enhanced the hydraulic permeability of the reservoir, leading to fluid migration out from it. This break of the fluid compartmentalization within the Madison–Phosphoria core is consistent with the geochemical data on the same fracture set that suggests a vertical fluid migration event within the sedimentary cover (Beaudoin et al., 2011). The review by Evans and Fischer (2012) indicates that compartmentalization of hydrologic reservoir may systematically ceases during folding, due to the vertical fluid migration related to development of syn-folding fracture set. After folding, the positive value of $\Delta\sigma_v$ suggests an exhumation of the strata, consistent with the development of the structural topography during folding. Considering that curvature-related fractures connected the Madison–Phosphoria reservoir with overlying shales formations, thus breaking the impermeable seal and triggering vertical fluid flow at the cover-scale (Fig. 6 h, Beaudoin et al., 2011), two hypotheses can be made (Fig. 5 a): either (1) a hydrostatic fluid pressure prevailed in the reservoir, in which case exhumation can be calculated about 1.3 km (Eq. (1)), or (2) a supra-hydrostatic fluid pressure persisted even after folding in the reservoir, in which case the syn-folding value of $\Delta\sigma_v$ (8 MPa) reflects the remaining fluid overpressure, and thus exhumation is calculated about 0.6 km (Eq. (1)).

Because the strata were more intensively affected by the early Sevier tectonics in the western part of the basin, the evolution of the values of $\Delta\sigma_v$ at RMA covers a larger timespan (Fig. 5 b). During Sevier tectonics, the evolution of $\Delta\sigma_v$ shows a decrease in fluid overpressure from the Sevier LPS-related fracture set S-I to the Sevier flexural forebulge related set S-II, where the value of 0 MPa is reached, revealing an hydrostatic pressure value, being also the minimum value reconstructed during history at the scale of RMA. Note that this decrease may not be as important as seemingly because of the large uncertainty on the value of $\Delta\sigma_v$ for set S-I. This uncertainty is due to the lack of information about the differential stress magnitude or even about the stress ellipsoid shape ratio (Φ), so in this strike-slip regime, σ_v may theoretically ranges from 0 MPa to the value of σ_h. After development of the flexure-related extensional fracture set, $\Delta\sigma_v$ exhibits an increase in fluid overpressure during the whole Sevier-LPS event, reaching a maximum value of 21 MPa that corresponds roughly to the lithostatic pressure at that depth (Figs. 5 b and 6). This increase can reflect destruction of porosity and/or a poor hydraulic permeability of joints, as in the case of SMA, but mechanical stratigraphy of strata differs, fractures being more vertically persistent at RMA than at SMA (Fig. 6 f, Barbier et al., 2012b). Moreover, because only very few Sevier-related stylolites are documented, this increase most likely reflects an input of exotic fluids flow in strata and fracture healing by precipitation of those fluids, as suggested by the palaeo-fluid system reconstruction in the very same veins (Beaudoin et al., 2014). In addition, it is worth noting that we consider a burial difference about 1 km between Sevier and Laramide times, corresponding to the thickness of the Cody Shale Fm deposited in between. Obviously, deposition was progressive during the upper Cretaceous and so the increase in $\Delta\sigma_v$ may also partially reflect an effect of the burial, so values from set S-III and Sevier LPS-4 must be considered carefully. Nevertheless, using the burial curves (Fig. 4), we can estimate that the deposition of the Cody Shale alone may account for an increase of the value of $\Delta\sigma_v$ up to 14 MPa, which is less that the total increase of $\Delta\sigma_v$ reconstructed, which implies in all cases an increase of fluid overpressure. An alternate explanation for the increase in fluid overpressure is to invoke the Sevier production of Paleozoic oil (Fox and Dolton, 1996). However, this remains unlikely because of the low burial of the strata (2–3 km considering the deposition of the Cody shales, Fig. 4) that is too low to produce important quantities of hydrocarbons, and also because no hydrocarbons–fluids interactions have been documented at RMA (Beaudoin et al., 2014).

During the Laramide compression, the uncertainty on $\Delta\sigma_v$ values during the LPS-3 deformation step due to uncertainty about the Φ parameter can be minimized. Indeed, the coeval development of both strike-slip and reverse faults at fold-scale suggests a stress regime close to the permutation between σ_v and σ_h (Beaudoin et al., 2012). Thus, we consider a ϕ ratio of 0.1 (Table A in supplementary material). The $\Delta\sigma_v$ evolution increases accordingly to the stress build-up from LPS-2 to LPS-3 steps, before decrease to the minimum value recorded during syn-folding. For the syn-folding value of $\Delta\sigma_v$, the same assumptions than in SMA may be done in RMA, so it is likely that the value of $\Delta\sigma_v$ recorded during folding reflects the fluid overpressure level and that exhumation can be still neglected at that step. The minimum of fluid overpressure level being reconstructed during this step is consistent with what is proposed at SMA (Fig. 6 h): the development of curvature-related fractures enhanced hydraulic permeability at cover-scale, triggering vertical fluid migration out from the reservoir, and so breaking the overlying/underlying seals. The late stage fold tightening provides the opportunity to estimate the syn-folding exhumation range considering a mean value of $\Delta\sigma_v$ for both limbs and by making two hypotheses as in the case of SMA: (1) an hydrostatic fluid pressure prevails in the reservoir, in which case exhumation is calculated about 2.0 km, (2) a supra-hydrostatic fluid pressure remains in the reservoir, in which case the value of $\Delta\sigma_v$ reconstructed for the syn-folding event (14 MPa) can be considered as reflecting the

remaining fluid overpressure, and thus exhumation is calculated about 0.8 km. The difference in the estimates of syn-folding exhumation between SMA and RMA is consistent with the difference in fold amplitudes (Fig. 1 d–e). It also supports that SMA reflects a juvenile state of Laramide basement-cored folding as already proposed by Katz et al. (2006) based on geochemical evidences and by Beaudoin et al. (2012) based on structural observations.

Robustness of estimates of the syn-folding erosion quantities can be tested by assuming a reasonable duration of folding and by comparing the inferred exhumation rates to exhumation/uplift rates derived from apatite fission-track data in various Laramide uplifts: Teton, Gros Ventre Range and Wind River Range (0.1–0.3 mm/yr during Late Cretaceous; Roberts and Burbank, 1993) and in the Beartooth Block (0.4–0.8 mm/yr from early Paleocene and early Eocene; Omar et al., 1994). To do such, we base our reasoning on estimates of fault-related folding rates in similar context, predicting the duration of folding to 1–8 Ma (Suppe et al., 1991). Assuming the syn-folding erosion between 0.6 km and 1 km for SMA and between 0.8 km and 2.0 km for RMA during 5–20 Ma (*i.e.* from the mean predicted value by Suppe et al. (1991) to the timespan from late Cretaceous to early Eocene, when most of the Laramide tectonics occurred) leads to a rough estimate of the exhumation rate by folding of about 0.03–0.20 mm/yr for SMA and 0.04–0.40 mm/yr for RMA. The consistency of these reconstructed exhumation rates with the one derived from apatite fission-tracks (Roberts and Burbank, 1993; Omar et al., 1994) tends to support the reconstruction we performed. In addition, the recent reconstruction of the subsidence history of the BHB based on stratigraphy from wells predicts an important tectonic uplift of the central part of the basin around 50 Ma (~1000 m, Fig. 4, May et al., 2013). Because this uplift is related to the development of the Laramide uplift (DeCelles, 2004), both the timing and amplitude of this tectonic uplift are consistent with the syn-folding exhumation that we reconstruct (Fig. 3), and so validate the approach adopted in this paper.

4.2. What are the mechanisms that govern the fluid overpressure evolution in the Madison–Phosphoria reservoir during Sevier–Laramide tectonics?

Once corrected for the effect of depth on the differential stress magnitudes reconstructed from calcite twinning, the evolution of $\Delta\sigma_v$ can be considered as reflecting fluid overpressure evolution until folding; values on each side of the basin can be compared and the evolution during the whole Sevier thin-skinned and Laramide thick-skinned tectonics can be followed (Fig. 7). The late stage fold tightening is not represented here because we cannot have a direct constraint about the depth of burial, and because the fluid overpressure level evolution cannot be assessed with certainty in that case. During the Sevier tectonics, the fracture sets mainly developed in the western part of the Bighorn Basin (Beaudoin et al., 2012). Consequently, the only time to compare RMA and SMA is during the development of LPS-related fracture set S-III, and one can observe a common fluid level pressure in the Madison–Phosphoria reservoir on each side of the basin (about 20 MPa).

Because fluid overpressure is possibly governed by specific parameters, it is possible to interpret the evolution of $\Delta\sigma_v$ regarding local-scale and basin-scale variations of these parameters. As mentioned earlier, these parameters are: the disequilibrium compaction (Nordgard Bolas et al., 2004); the fluid generation in the reservoir by both hydrocarbon production (Becker et al., 2010) or smectite dehydration (Yassir and Bell, 1996); the migration of fluids in and out the reservoir related to hydraulic permeability of overlying and underlying formations (e.g. Bruhn et al., 2000); the destruction of porosity in carbonates, and more generally stress evolution (e.g. Yassir and Bell, 1996; Roure et al., 2010). Thus, evolution of fluid overpressure is directly related to the burial,

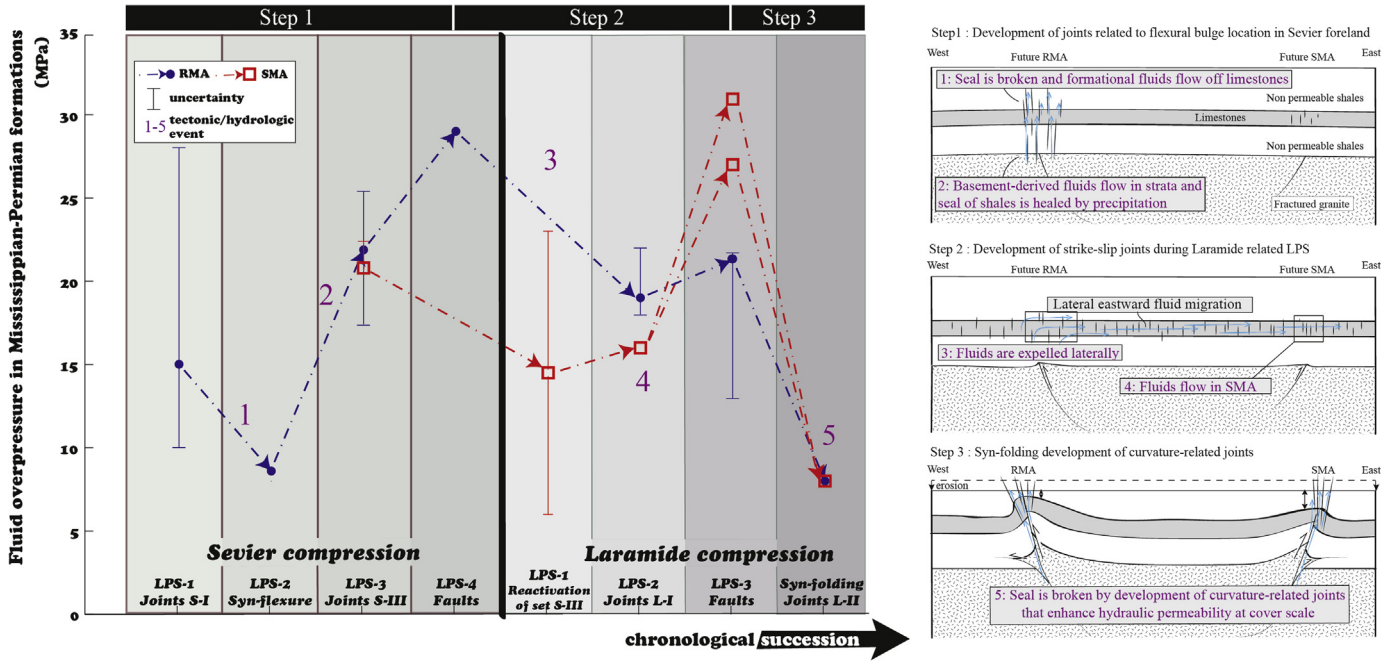

Figure 7. Fluid overpressure evolution during Sevier and Laramide tectonics and stress build-up at RMA (blue dots) and SMA (red squares) (right-hand of the figure). Values are corrected from effect of depth on the differential stress and are normalized to the depth of 2 km (corresponding to the overburial of SMA during Laramide tectonics). Labels 1–5 are related to fluid migration events 1–5 illustrated on the schematic cross section at basin-scale (left-hand of the figure) reporting the main phases of evolution of the Bighorn basin from the flexural bulge to Laramide development of SMA and RMA. (For interpretation of the references to color in this figure legend, the reader is referred to the web version of this article.)

tectonics, and mechanical stratigraphy of strata and to the hydraulic permeability of fracture sets. Such information is partly available from previously published studies. Indeed, data from fracture population development at basin-scale (Bellahsen et al., 2006a,b; Amrouch et al., 2010a, b; Beaudoin et al., 2012), palaeofluid system evolution (Beaudoin et al., 2011, 2013) and mechanical stratigraphy (Barbier et al., 2012a,b) allow discussing what parameters likely controlled the fluid overpressure evolution in the Madison–Phosphoria reservoir. Again, because of the location of the studied folds on both edges of the basin, disequilibrium compaction most probably did not develop fluid overpressure, as the volume of sediments deposited in these places is negligible (Thomas, 1965; DeCelles, 2004). The lithology of strata and limited burial depth also excludes smectite-illite transformation as a significant source of fluid. Thus, the evolution of fluid overpressure can be related either to horizontal stress evolution (Yassir and Bell, 1996) or to fluid flow migration in and out the Madison–Phosphoria Reservoir (Bruhn et al., 2000).

Interpretation of this fluid overpressure evolution at fold and basin-scale in term of fluid migration is made possible by the independent fluid system reconstruction done at these scales (Katz et al., 2006; Beaudoin et al., 2011; Barbier et al., 2012a,b; Beaudoin et al., 2014). Based on a complete and consistent geochemical dataset gathering O, C and Sr stable isotopes, and fluid inclusion microthermometry and chemistry, the most complete scenario of fluid system evolution can be summarized as a mainly vertically closed and laterally stratified (*sensu* Fischer et al., 2009) fluid system except during two main tectonic events. These two events are witnessed by specific fracture set (set S-II and L-II) in which cements are characterized by (1) homogeneous and very depleted $\partial^{18}O$ signatures, (2) high temperature and a zero salinity, (3) a more radiogenic $^{87/86}Sr$ signatures regarding other cements from the same structures, and (4) depleted $\partial^{13}C$ signatures in the eastern part of the BHB only. Thus, the scenario proposed that during forebulge-related flexure (set S-II), hydrothermal fluids of meteoric origin were remobilized from depth (where they were in contact with the basement rocks, according to $^{87/86}Sr$ signatures) and migrated and precipitated as a fast vertical pulse in the set S-II fractures. This event affected only the western part of the BHB (RMA) and is followed by an eastward lateral and stratified migration of these fluids at basin-scale during all the Sevier and Laramide LPS deformation (sets S-III, L-0, L-I). The second phase with a fluid system open to such a vertical pulse of hydrothermal fluids was during the folding and strata curvature (set L-II). This event of vertical migration seems to be limited in space to a narrow zone striking parallel to the current hinge of the fold, suggesting that the underlying basement-fault played also an important role in this hydrothermal fluid migration (Beaudoin et al., 2011). Thus, basement cored fault seemingly affected the fluid system of the Madison–Phosphoria reservoir only during the syn-folding event. Also, the depleted $\partial^{13}C$ signatures that characterize the opening of the fluid system in the east part of the basin have been related to mixing with hydrocarbons. In both events, the fracture development is believed to have enhanced the vertical permeability by breaking the seals underlying and overlying the reservoir, which is required to allow a fast vertical fluid migration. These three steps are reported on Figures 6 and 7.

Independently, we define three major stages depicting overall trends of fluid overpressure evolution and 5 structural events affecting more specifically the evolution at fold-scale (Fig. 7). The early decrease in fluid overpressure during the opening of the flexure-related joint sets (Fig. 7, step 1, event 1) might reflect an exhaust of fluids from the reservoir, likely related to the development of highly vertically permeable fracture set S-II (Beaudoin et al., 2014). However, this early evolution is poorly constrained due to the uncertainty on the LPS-1 value. The subsequent increase in fluid overpressure in the reservoir (Fig. 7, step 1, event 2) can be related to fracture healing by precipitation of calcite which reduces the overall permeability. As mentioned before, this increase might be maximized because our estimates do not consider the poorly defined burial during Cretaceous due to the Cody Shale deposition. Nevertheless, this 1 km burial alone cannot explain the total increase during this event 2. Considering that the pulse of basement-derived fluids has been depicted only in the western part of the basin during flexure (Beaudoin et al., 2014), the similar fluid overpressure level at the basin scale suggests that this input of exotic fluids poorly impacted the fluid overpressure before Sevier LPS-4, and so the level of overpressure about 20 MPa reached during Sevier LPS-3 is likely the initial level of fluid overpressure in the reservoir, so witnessing a fast healing of set S-II joints by fluid precipitation. The difference in fluid overpressure level during the Sevier LPS-4 at the basin scale is related to the development of Sevier reverse faults mainly in the western part of the basin, closer to the front of the Sevier belt (Beaudoin et al., 2012). The high overpressure level sustained at that time in the western part of the basin is clearly coeval with the compressional stress build-up, which may affect fluid overpressure in sealed reservoirs (e.g. Yassir and Bell, 1996). This high overpressure reflects the fact that the development of small-scale reverse faults did not trigger exhaust of fluids out of the Madison–Phosphoria reservoir.

Step 2 extends from the high level of overpressure at the climax of Sevier-related stress build-up to the end of the Laramide LPS, when the climax of Laramide-related stress build-up affected strata (Beaudoin et al., 2012). This step can be sub-divided in three events, starting with an overall decrease of fluid overpressure at fold-scale. It is noteworthy that the amplitude of the decrease is twice more important at RMA than at SMA (Fig. 6, step 2, event 3). During this event, an important decrease in horizontal stress magnitude occurred at RMA (Beaudoin et al., 2012) while σ_H magnitude was rather constant at SMA (Amrouch et al., 2011). Thus, if related to stress, this difference in fluid overpressure supports the stress attenuation during transmission from the Sevier deformation front located west of the BHB, as proposed recently (Beaudoin et al., 2012). Other events can explain that this decrease in fluid overpressure is more important in the western part of the basin. Indeed, the paleohydrological model reconstructed for the BHB during Sevier–Laramide tectonics proposed large-scale eastward fluid migrations (Bethke and Marshak, 1990; Barbier et al., 2012b; Beaudoin et al., 2014). In a laterally connected formation as the Phosphoria–Madison reservoir, fluid pressure can be transferred by fluid migration until pressure equilibrium is reached at basin scale (e.g. Michael and Bachu, 2001). This equilibrium can be considered as prevailing during the Laramide LPS-2 deformation event (Fig. 7, step 2, event 4). The pressure disequilibrium between the eastern and the western part of the basin during late Sevier and early Laramide times can have acted as a driving force for the eastward migration, at a rate of about 8 km/Ma (Beaudoin et al., 2014). Note that the little increase of fluid overpressure at SMA between Laramide LPS-1 and LPS-2 is neglected when interpreting the overall trends at basin-scale, which is consistent with the lack of variation of principal stress magnitudes at SMA. To account for this increase, the difference in the vertical persistence of fractures from Sevier to Laramide sets observed in the Mississippian Madison Fm. from west to east (Barbier et al., 2012a,b) might be invoked, fractures from set L-1 potentially triggering less vertical fluid migration out from the reservoir by breaking the overlying sealing formations in the east than in the west. At the same time, the reduction of porosity in limestones by pressure-solution affected the eastern part of the basin (Amrouch et al., 2010a, 2011) and consequently,

fluid overpressure level in strata at SMA increased while it decreased at RMA.

Once pressure equilibrium is reached in strata (Fig. 7, event 4), it is likely that large-scale fluid migration stopped. Even if fluid migration continued, driven by other driving forces (as a thermal or hydraulic gradients), it should have weakly affected the fluid pressure anymore. The late Laramide LPS-3 evolution of fluid overpressure is similar at each fold-scale, with an increase consistent with stress build-up and local stress perturbation (at SMA, Amrouch et al., 2011).

During Laramide folding, the fluid overpressure decreased both at RMA and SMA down to a minimum level (Fig. 7, step 3), which suggests a common mechanism that broke the overlying seal. This decrease is likely related to the high hydraulic permeability of curvature-related extensional fracture sets (Fig. 7, event 5), which supports that these fracture sets would have triggered cover-scale vertical fluid migration as depicted at SMA (Beaudoin et al., 2011). It is also consistent with the recent overview of fluid system evolution in folds during deformation that points out that curvature-related joints and fractures systematically break seals and connect reservoirs vertically, thus triggering fluid migrations (Evans and Fischer, 2012). This suggests that the curvature related joints from set L-II may also have triggered efficient vertical fluid migration at RMA. However, there the hinge is eroded and the geochemical dataset is scarce regarding this event (Beaudoin et al., 2014).

The main difference between SMA and RMA is the timing of the maximum overpressure, lithostatic in these cases: Sevier at RMA and Laramide at SMA (Fig. 7). This contradicts previous conceptual models that relate the development of bed-perpendicular veins to burial occurring early during the LPS phase (Van Geet et al., 2002). The relation between burial and bed-perpendicular veins development is not supported by the fluid overpressure evolution reconstructed in our study, because during the Laramide tectonics the lithostatic pressure level is reached at SMA while no burial occurred at that time (DeCelles, 2004).

One striking result of this study is that reverse faults in the cover developed when fluid pressure was nearly-lithostatic (end of step 1 and 2), before folding related fracture sets triggered vertical fluid migrations, as in SMA. As depicted in previous studies (Katz et al., 2006; Beaudoin et al., 2011, 2013), the involved fluids migrated in the basement rocks, being likely channelized in fault zones. Thus, one can wonder if comparable fluid overpressure could have prevailed at this time, triggering reactivation of inherited possibly normal faults (Marshak et al., 2000; Erslev and Koenig, 2009) in poorly porous basement rocks. Even though our dataset reflects only fluid pressure values and evolution trends in the Madison–Phosphoria reservoir and cannot be extrapolated to the fluid pressure in the basement, it could be of interest to also constrain fluid overpressure in the basement rocks to assess whether fluid overpressure could have played a significant role in basement fault inversion and whether such results could help reconstruct crustal/lithospheric scale structural evolution of the area (e.g. Siddoway et al., 2011).

4.3. Lessons from the study of fluid pressure evolution in the Madison–Phosphoria limestone reservoir

In many natural cases, hydrostatic gradient prevails in strata, and some oil-producing basins are the location of underpressure reservoirs (e.g. Hao et al., 2012). However, the case study of Madison–Phosphoria reservoir is an interesting example to assess the problem of the fluid overpressure evolution in deforming media. It grants the opportunity to bring quantitative constraints on fluid pressure values that can be compared to natural datasets obtained thanks to hydrocarbon-bearing fluid inclusion modeling or currently measured in boreholes. Such comparison can help (1) validate the range of fluid (over)pressure values obtained using our method, (2) assess what parameters dominantly control fluid (over)pressure in sedimentary basins, (3) discuss whether subseismic fracture sets that developed at fold-/basin-scale are well-suited objects to reconstruct large-scale fluid pressure evolution in strata. Comparison with abnormally pressured sandstone reservoirs will also led to consider the role of host-rock nature and how permeability/porosity of strata influence the fluid (over) pressure.

4.3.1. Fluid overpressure evolution in the Madison–Phosphoria reservoir regarding other natural data on fluid pressure in basins

Available estimates of fluid overpressures in sedimentary basins (Fig. 8) come from paleo-pressure reconstructions based on gas composition in hydrocarbons fluid inclusions (Becker et al., 2010; Fall et al., 2012) or from direct measurements in various reservoirs from basins consisting of either limestones (Hunt, 1990) or shales/sandstones (Yu and Lerche, 1996; Bruhn et al., 2000; Nordgard Bolas et al., 2004; Van Ruth et al., 2004). An envelope of fluid pressure prevailing in non-overpressured zones of basins is also reported on Figure 8.

The lithostatic pressure gradient considering a mean sedimentary rock density of 2.4 and the hydrostatic pressure gradient have been drawn in Figure 8. The blue dotted line is the linear regression according to overpressure data currently measured in abnormally pressured limestone reservoirs (Hunt, 1990). The high value of the regression factor ($r = 0.95$) exhibits the strong correlation of overpressure with depth (blue dotted line, Fig. 8). This line is called Mean Overpressure Level (MOL) hereinafter. We also reported our estimates of fluid pressure during the evolution of the BHB, at each step of the deformation and with respect to the reconstructed burial depths.

The supra-hydrostatic pressure condition that prevails in many sedimentary basins (Fig. 8) is classically related to the production of gas and hydrocarbons in the rock reservoirs (Yassir and Bell, 1996; Fall et al., 2012) or to disequilibrium compaction (Yu and Lerche, 1996; Roure et al., 2010). Our fluid pressure estimates for SMA and RMA suggest that a supra-hydrostatic fluid pressure level prevails at any time of the deformation of the BHB, whatever this evolution involves hydrocarbon generation or not. Considering either LPS-related joint development or reactivation, our fluid pressure estimates line up well with the mean overpressure level reconstructed from the current measurement in comparable reservoirs (Hunt, 1990), suggesting a common overall behavior of fluid pressure in limestone reservoirs overlain by non-permeable seals. In the case of the studied folds, it is striking that LPS-related reverse faults systematically developed when a nearly lithostatic fluid pressure level was reached in strata, and this occurred at the end of Sevier LPS stage at RMA and at the end of Laramide LPS stage at SMA, when the differential stress and σ_H magnitudes are the highest in the deformation history. This result is consistent with previous models and observations that led Sibson (1989, 2004) to conclude that a supra-hydrostatic fluid pressure is easy to sustain and so usually encountered in compressional settings. As a high fluid overpressure prevails in strata during reverse fault development, the reverse faults do not seem to trigger fluid exhaust off the reservoir, suggesting that the development of faults is tectonically-driven rather than hydraulically-driven. It is worth nothing that this high overpressure level that could overcome the lithostatic value is witnessed by the development of bed-perpendicular veins at SMA, likely driven by fluid pressure (Amrouch et al., 2010a), and this is in agreement with findings in other basins from the Sevier-Laramide foreland (Fall et al., 2012).

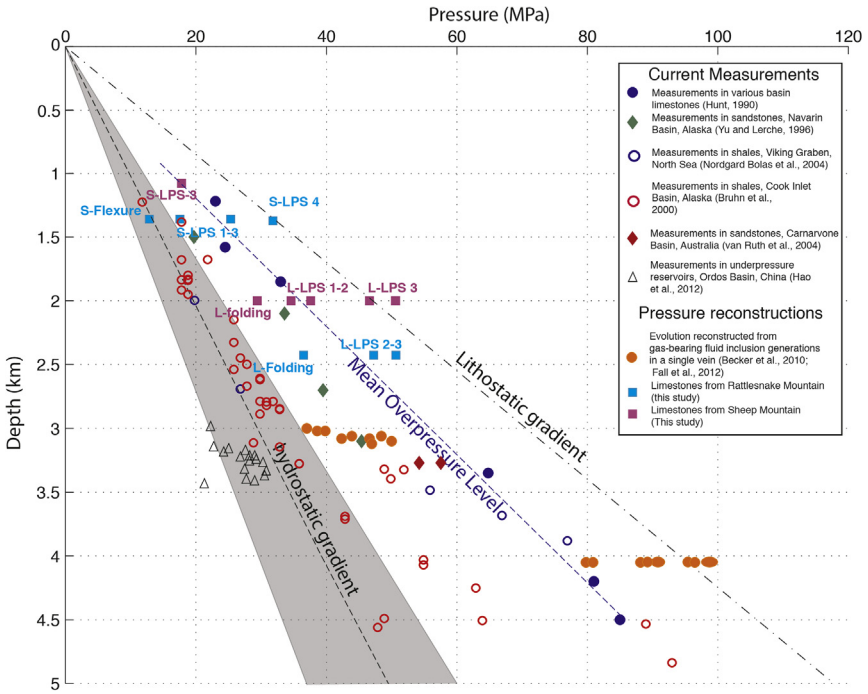

Figure 8. Pressure vs depth plot of various measured and reconstructed data from the literature (Hunt, 1990; Yu and Lerche, 1996; Bruhn et al., 2000; Nordgard Bolas et al., 2004; Van Ruth et al., 2004; Becker et al., 2010; Fall et al., 2012; Hao et al., 2012) and of pressure data from this study, regarding the deformation phase. Orange and blue squares represents data acquired in this study, from SMA and RMA, respectively. Each step of deformation at which fluid overpressure have been reconstructed is reported alone. Hydrostatic and lithostatic gradients are reported on the plot, and blue dotted line is a linear regression on mean measured data in overpressure limestone reservoirs in compressive basins (Hunt, 1990), symbolizing the mean overpressure level in limestones in active tectonics sedimentary basins. (For interpretation of the references to color in this figure legend, the reader is referred to the web version of this article.)

Fluid overpressure levels attained during development of flexure and folding-related fracture sets are the lowest among our reconstructions, being below the mean overpressure level. During the lithospheric curvature related to forebulge development, fluid pressure is even hydrostatic, and it is noteworthy that this is only during this step that the reservoir is not overpressured (Fig. 8). These fracture sets differs from those formed during other deformation stages because they developed under extensional stress regimes, and because the lower fluid overpressure level reached suggests a higher hydraulic permeability (Beaudoin et al., 2014). Overpressure data during extensional vein opening reconstructed using gas-bearing fluid inclusions in the Cretaceous Travis Peak formation exhibit also a supra-hydrostatic fluid pressure that is below the mean overpressure level (Fig. 8, Becker et al., 2010). This supports that fluid overpressure in carbonate strata is related to vertical hydraulic permeability of fractures and that joints formed under an extensional stress regime efficiently triggered fluid exhaust leading to fluid overpressure decrease (Sibson, 2004). This result is consistent with the recent observation that curvature-related fracture sets trigger vertical fluid migration in folds, connecting together previously stratified reservoirs (e.g. Evans and Fischer, 2012).

The fluid overpressure values reached in compressional basins mainly filled up with sandstones and shales (Yu and Lerche, 1996; Bruhn et al., 2000) slightly differ from our dataset and from the data available in other limestone reservoirs undergoing compressional stresses (Hunt, 1990; Fall et al., 2012). Indeed, fluid overpressure levels from these sandstone reservoirs are closer to the level reached during flexure or folding in limestone reservoirs (Fig. 8).

4.3.2. Are sub-seismic fracture populations good indicators for larger-scale fluid pressure evolution?

Diffuse population of sub-seismic fractures are interesting markers to be studied in order to reconstruct the stress and strain history and the evolution of the fluid system because (1) they are accessible, (2) they form a diffuse pattern at the fold scale, and (3) they developed before, during and after folding event, whereas fault zones preferentially record the main deformation events and large-scale fluid flows (e.g. Beaudoin et al., 2013). Thus, to assess the question of fluid pressure evolution during deformation, the well-constrained and accurate time frame and the large-scale spatial coverage offered by diffuse sub-seismic fracture sets are well suited. Nevertheless, questions about the timing of fracture development must be addressed when we reconstruct the fluid pressure level that prevails in strata based on the analyses of the cements precipitated from these fluids. In this study, we consider that joint sets developed over a time-span corresponding to the duration of the tectonic stage responsible for their opening. This consideration is based on the assumption that joints develop rapidly compared to other transformations in rocks (Lash and Engelder, 2007), but some doubts about this classical assumption have recently raised (Becker et al., 2010 and references herein). Indeed, the evolution of the fluid pressure though time as recorded in a single vein from the Cretaceous Travis Peak Fm (Texas, USA) and the comparison with subsidence-exhumation reconstructions suggest that this vein opened during 48 My (Becker et al., 2010). This estimate is based on gas bearing pseudo-secondary fluid inclusion populations trapped in successive quartz cements that represent successive growth phases. Pseudo-secondary fluid inclusion trails being parallel to the vein, authors use them as indicators of how pressure and temperature evolved during vein opening, without any regard to the tectonics that triggered vein development or to the mechanisms that triggered quartz precipitation from fluid. In the active tectonic context of the Bighorn Basin, it is unlikely that fracture sets could witness a really long time of opening for several reasons: (1) fracture sets present systematic consistent chronological relationships at fold-scale, and a

distribution that is clearly related to fold/basement fault development (Bellahsen et al., 2006a; Amrouch et al., 2010a) and/or to large-scale tectonics (Beaudoin et al., 2012). Moreover, some of these fracture sets are documented in several structures of the basin, exhibiting chronological relationships consistent at this scale. This observation also shows that diffuse fracture populations are good markers to reconstruct successive regional stress fields. Thus, in most cases formation or reactivation of a fracture set may be limited in time by the event predating or postdating it. (2) Strain and stress reconstructions from calcite twins and fault slip data inversion reveal multiple stages of fracture formation/reactivation and related states of stress. Sequential deformation and paleostress reconstructions are carried out from both veins and host rocks, supporting the chronological relationships deciphered at fold-scale. The recognized deformation stages being often related to transient stress regimes in the fold history, it is really unlikely that a fracture can be opening longer than the duration of the tectonic event. (3) Previous works discussed the mechanism that triggered calcite precipitation in vein in the case of SMA and RMA (Beaudoin et al., 2011; Evans and Fischer, 2012; Beaudoin et al., 2014). In all these works, the invoked mechanism is directly related to joint opening, which means that the fast precipitation occurred as soon as the joint opened either by the development of pressure gradient, or by mixing between different fluids. Thus, if we consider that fracture opening covered a long timespan, we must consider a mechanism allowing very slow precipitation of calcite from fluids, as in the reconstruction of Becker et al. (2010) at about 16–23 μm/My. In the case of folds from the BHB, a slow precipitation rate is contradicted by the geochemical dataset that strongly suggest fast migration and precipitation mechanisms (Beaudoin et al., 2011, 2014).

These arguments therefore tend to validate the assumption that in the case of the Bighorn basin, tectonic-driven fracture sets opened rapidly relative to other rock transformations (as proposed by Lash and Engelder, 2007). Considering that cement precipitation in a vein occurred during its early opening, reconstruction of $\Delta\sigma_v$ based on mean values of differential stress obtained from cements from both veins and host rock must theoretically represent the mean fluid overpressure prevailing in the strata during the fracture set development. Thus, it is valid to discuss fluid overpressure evolution during deformation based on mean overpressure values that prevailed during successive specific tectonic stages. It is also valid to consider a progressive evolution of fluid pressure over time like that presented herein (Figs. 5 and 7) rather than to consider that fluid pressure level remained the same during all the tectonic stages, followed by sudden changes in fluid pressure in strata. The latter appears equivalent to consider that all fractures from the same fracture set developed at fold-scale perfectly at the same time, which is unlikely. Moreover, by considering mean values and graduate evolution of fluid pressure for and between each deformation event, we can upscale data at the scale of the entire basin even if sub-seismic fracture set did not develop coevally within each part of the basin. This discussion is also possible because studied folds have similar structural evolution, and because the Laramide deformation likely did not propagate from west to east at the basin-scale, the easternmost Laramide arches (the Bighorn Mountains) being exhumed early in the Laramide history. Thus, it is reasonable to assume that the development of folds and related structures was coeval at basin-scale, and so that the comparison of Laramide fluid overpressures evolutions from fold to fold is sound.

5. Conclusion

Using analytical data, we present quantitative reconstruction of the evolution of fluid overpressure during successive deformation stages related to fold development and stress build-up in the compressional Bighorn Basin. The interpretation of this evolution suggests a major impact of vertical and lateral permeability due to fracture development, allowing large-scale fluid migrations that partially impact the local-scale fluid pressure evolution. In addition, the validity of our method for quantifying fluid overpressure is supported by the comparison with other reconstructed or measured fluid pressure values in similar geological and sedimentary settings.

Along with a paleohydrological model, suggesting that the Madison–Phosphoria reservoir was connected at the basin-scale during the Sevier–Laramide tectonics, our study of the fluid overpressure evolution shows that among factors controlling fluid overpressure in basins, stress magnitude, large-scale fluid migrations and hydraulic permeability of both reservoir and over-/underlying seals seem to dominate over fluid generation or disequilibrium compaction, as classically suggested in sedimentary basins (Yu and Lerche, 1996; Yassir and Bell, 1996: Nordgard Bolas et al., 2004; Becker et al., 2010). It points out that at least until after folding, a supra-hydrostatic fluid pressure prevails in strata, supporting the previous observations that fluid overpressures are easy (easier) to sustain in compressional tectonic regimes (Sibson, 2004). This study also reveals that fluid overpressure evolution is similar during Sevier thin-skinned and Laramide thick-skinned tectonics, suggesting that fluid pressure evolution should be more or less independent on the tectonic style, even though the latter directly impacted stress evolution, fracture development and fluid migrations in the Bighorn Basin (Beaudoin et al., 2012, 2014). Extensional stress regimes, driven either by regional foreland flexure or local strata curvature at fold hinges, lead to a decrease in fluid overpressure that get closer to the values recorded in sandstone reservoirs, underlining the impact of porosity and permeability of host rocks on the overpressure levels. Joint sets that developed under extensional stress regime strongly impacted rock hydraulic permeability and triggered fluid migrations in and out the overpressured reservoir. Indeed, this fracture type (curvature/flexure-related) is more efficient to release fluid overpressure than strike-slip/reverse faults that in contrast preferentially developed when fluid overpressure reaches the lithostatic pressure, just before or coevally with formation of bedding-parallel veins. This observation supports the recent overall statement about the role of curvature (*sensu largo*)-related joint sets on fluid migration during strata folding (e.g. Evans and Fischer, 2012).

Acknowledgments

This work was funded by the Institut des Sciences de la Terre de Paris (ISTeP, UPMC Paris 6, France). Authors thank F. Roure, R. Swennen, and an anonymous reviewer for their high-quality reviews that greatly improve the original manuscript.

Appendix A. Supplementary data

Supplementary data related to this article can be found at http://dx.doi.org/10.1016/j.marpetgeo.2013.12.009.

References

Amrouch, K., Beaudoin, N., Lacombe, O., Bellahsen, N., Daniel, J.-M., 2011. Paleostress magnitudes in folded sedimentary rocks. Geophys. Res. Lett. 38, 2–7. L17301.
Amrouch, K., Lacombe, O., Bellahsen, N., Daniel, J.-M., Callot, J.-P., 2010a. Stress and strain patterns, kinematics and deformation mechanisms in a basement-cored anticline: Sheep Mountain Anticline, Wyoming. Tectonics 29, 1–27. TC1005.
Amrouch, K., Robion, P., Callot, J.-P., Lacombe, O., Daniel, J.-M., Bellahsen, N., Faure, J.-L., 2010b. Constraints on deformation mechanisms during folding provided by rock physical properties: a case study at Sheep Mountain anticline (Wyoming, USA). Geophys. J. Int. 182, 1105–1123.

Barbier, M., Hamon, Y., Callot, J.-P., Floquet, M., Daniel, J.-M., 2012a. Sedimentary and diagenetic controls on the multiscale fracturing pattern of a carbonate reservoir: the Madison Formation (Sheep Mountain, Wyoming, USA). Mar. Pet. Geol. 29, 50–67.

Barbier, M., Leprêtre, R., Callot, J.-P., Gasparrini, M., Daniel, J.-M., Hamon, Y., Lacombe, O., Floquet, M., 2012b. Impact of fracture stratigraphy on the paleohydrogeology of the Madison Limestone in two basement-involved folds in the Bighorn Basin, (Wyoming, USA). Tectonophysics 576–577, 116–132.

Beaudoin, N., Bellahsen, N., Lacombe, O., Emmanuel, L., 2011. Fracture-controlled paleohydrogeology in a basement-cored, fault-related fold: Sheep Mountain Anticline, Wyoming, United States. Geochem. Geophys. Geosyst. 12, 1–15.

Beaudoin, N., Lacombe, O., Bellahsen, N., Emmanuel, L., 2013. Contribution of studies of sub-seismic fracture populations to paleo-hydrological reconstructions (Bighorn Basin, USA). Proc. Earth Planet. Sci. 14 (7), 57–60. http://dx.doi.org/10.1016/j.proeps.2013.03.198. Water Rock Interaction.

Beaudoin, N., Bellahsen, N., Lacombe, O., Emmanuel, L., Pironon, J., 2014. Crustal-scale fluid flow during the tectonic evolution of the Bighorn Basin (Wyoming, USA). Basin Res.. http://dx.doi.org/10.1111/bre.12032.

Beaudoin, N., Leprêtre, R., Bellahsen, N., Lacombe, O., Amrouch, K., Callot, J.-P., Emmanuel, L., Daniel, J.-M., 2012. Structural and microstructural evolution of the Rattlesnake Mountain Anticline (Wyoming, USA): new insights into the Sevier and Laramide orogenic stress build-ups in the BigHorn Basin. Tectonophysics 576-577, 20–46.

Becker, S.P., Eichhubl, P., Laubach, S.E., Reed, R.M., Lander, R.H., Bodnar, R.J., 2010. A 48 m.y. history of fracture opening, temperature, and fluid pressure: Cretaceous Travis Peak Formation, East Texas basin. Geol. Soc. Am. Bull. 122, 1081–1093.

Bellahsen, N., Fiore, P., Pollard, D., 2006a. The role of fractures in the structural interpretation of Sheep Mountain Anticline, Wyoming. J. Struct. Geol. 28, 850–867.

Bellahsen, N., Fiore, P.E., Pollard, D.D., 2006b. From spatial variation of fracture patterns to fold kinematics: a geomechanical approach. Geophys. Res. Lett. 33, 1–4.

Bethke, C., Marshak, S., 1990. Brine migrations across North America – the plate tectonics of groundwater. Annu. Rev. Earth Planet. 18, 287–315.

Bons, P.D., Elburg, M.A., Gomez-Rivas, E., 2012. A review of the formation of tectonic veins and their microstructures. J. Struct. Geol. 43, 33–62.

Bour, O., Lerche, I., 1994. Numerical modelling of abnormal fluid pressures in the Navarin Basin, Bering Sea. Mar. Pet. Geol. 11, 491–500.

Bourdet, J., Eadington, P., Volk, H., George, S.C., Pironon, J., Kempton, R., 2012. Chemical changes of fluid inclusion oil trapped during the evolution of an oil reservoir: Jabiru-1A case study (Timor Sea, Australia). Mar. Pet. Geol. 36, 118–139.

Bruhn, R.L., Parry, W.T., Bunds, M.P., 2000. Tectonics, fluid migration, and fluid pressure in a deformed forearc basin, Cook Inlet, Alaska. GSA Bull. 112 (4), 550–563.

Cobbold, P.R., Durand, S., Mourgues, R., 2001. Sandbox modelling of thrust wedges with fluid-assisted detachments. Tectonophysics 334, 245–258.

Cobbold, P.R., Mourgues, R., Boyd, K., 2004. Mechanism of thin-skinned detachment in the Amazon Fan: assessing the importance of fluid overpressure and hydrocarbon generation. Mar. Pet. Geol. 21, 1013–1025.

Cobbold, P.R., Zanella, A., Rodrigues, N., Løseth, H., 2013. Bedding-parallel fibrous veins (beef and cone-in-cone): worldwide occurrence and possible significance in terms of fluid overpressure, hydrocarbon generation and mineralization. Mar. Pet. Geol. 43, 1–20.

Cornet, F.H., Bérard, T., Bourouis, S., 2007. How close to failure is a granite rock mass at a 5 km depth? Int. J. Rock Mech. Min. Sci. 44, 47–66.

Cornet, F.H., Doan, M.L., Fontbonne, F., 2003a. Electrical imaging and hydraulic testing for a complete stress determination. Int. J. Rock Mech. Min. Sci. 40, 1225–1241.

Cornet, F.H., Li, L., Hulin, J.-P., Ippolito, I., Kurowski, P., 2003b. The hydromechanical behaviour of a fracture: an in situ experimental case study. Int. J. Rock Mech. Min. Sci. 40, 1257–1270.

Cornet, F.H., Morin, R.H., 1997. Evaluation of hydromechanical coupling in a granite rock mass from a high-volume, high-pressure injection experiment: Le Mayet de Montagne, France. Int. J. Rock Mech. Min. Sci. 34, 207.

Craddock, J., Van der Pluijm, B.A., 1999. Sevier–Laramide deformation of the continental interior from calcite twinning analysis, west-central North America. Tectonophysics 305, 275–286.

Crowley, P.D., Reiners, P.W., Reuter, J.M., Kaye, G.D., 2002. Laramide exhumation of the Bighorn Mountains, Wyoming: an apatite (U-Th)/He thermochronology study. Geology 30, 27.

DeCelles, P.G., 2004. Late Jurassic to Eocene evolution of the cordilleran thrust belt and foreland basin system, Western U.S.A. Am. J. Sci. 304, 105–168.

Dickinson, W.R., Klute, M.A., Hayes, M.J., Janecke, S.U., Lundin, E.R., McKittrick, M.A., Olivares, M.D., 1988. Paleogeographic and paleotectonic setting of Laramide sedimentary basins in the central Rocky Mountain region. Geol. Soc. Am. Bull. 100, 1023–1039.

Douglas, T.A., Chamberlain, C.P., Poage, M.A., Abruzzese, M., Shultz, S., Henneberry, J., Layer, P., 2003. Fluid flow and the Heart Mountain fault: a stable isotopic, fluid inclusion, and geochronologic study. Geofluids 3, 13–32.

Durdella, M.J., 2001. Mechanical Modeling of Fault-related Folds: West Flank of the Bighorn Basin. Purdue University, Wyoming (M.S. thesis).

Erslev, E.A., 1995. Heterogeneous Laramide deformation in the Rattlesnake Mountain Anticline, Cody, Wyoming. Field Trip 7, 141–150.

Erslev, E.A., Koenig, N., 2009. Three-dimensional kinematics of Laramide, basement-involved Rocky Mountain deformation, USA: insights from minor faults and GIS-enhanced structure maps. GSA Memoirs 204, 125–150.

Etchecopar, A., 1984. Étude des états de contraintes en tectonique cassante et simulation de déforamtions plastiques. France, Montpellier, p. 270 (PhD thesis).

Evans, M.A., Fischer, M.P., 2012. On the distribution of fluids in folds: a review of controlling factors and processes. J. Struct. Geol. 44, 2–24.

Fall, A., Eichhubl, Peter, Cumella, S.P., Bodnar, Robert J., Laubach, Stephen E., Becker, Stephen P., 2012. Testing the basin-centered gas accumulation model using fluid inclusion observations: southern Piceance Basin, Colorado. AAPG Bull. 96, 2297–2318.

Finn, T.M., Kirschbaum, M.A., Roberts, S.B., Condon, S.M., Roberts, L.N.R., Johnson, R.C., 2010. Cretaceous – Tertiary Composite Total Petroleum System (503402), Bighorn Basin, Wyoming and Montana. In: U.S. Geological Survey Digital Data Series DDS–69–V, p. 157.

Fischer, M.P., Higuera-Díaz, I.C., Evans, M.A., Perry, E.C., Lefticariu, L., 2009. Fracture-controlled paleohydrology in a map-scale detachment fold: insights from the analysis of fluid inclusions in calcite and quartz veins. J. Struct. Geol. 31, 1490–1510.

Fox, J.E., Dolton, G.L., 1996. Petroleum geology of the central of the Bighorn Basin north-central Wyoming and south-central Montana. Wyoming Geological Association Guidebook 47, 19–39.

Hao, X., Jungfeng, Z., Dazhen, T., Ming, L., Wenzhong, Z., Wenji, L., 2012. Controlling factors of underpressure reservoirs in the Sulige gas field, Ordos Basin. Pet. Explor. Dev. 39 (1), 70–74.

Harris, J.F., Taylor, G.L., Walper, J.L., 1960. Relation of deformational fractures in sedimentary rocks to regional and local structures. AAPG Bull. 44, 1853–1873.

Hennier, J.H., 1984. Structural Analysis of the Sheep Mountain Anticline. Texas A&S University, Bighorn Basin, Wyoming, p. 118.

Hunt, J.M., 1990. Generation and migration of petroleum from abnormally pressured fluid reservoirs. AAPG Bull. 74, 1–12.

Jaeger, J.C., Cook, N.G.W., 1969. Fundamental of Rock Mechanics. Chapman and Hall, New York, p. 513.

Johnson, G.D., Garside, L.J., Warner, A.J., 1965. A study of the structure and associated features of Sheep Mountain Anticline, Big Horn County, Wyoming. Iowa Acad. Sci. 72, 332–342.

Katz, D.A., Eberli, G.P., Swart, P.K., Smith, L.B., 2006. Tectonic-hydrothermal brecciation associated with calcite precipitation and permeability destruction in Mississippian carbonate reservoirs, Montana and Wyoming. AAPG Bull. 90, 1803–1841.

Koch, P., Zachos, J., Dettman, D., 1995. Stable isotope stratigraphy and paleoclimatology of the Paleogene Bighorn Basin (Wyoming, USA). Palaeogeogr. Palaeoclimatol. 115, 61–89.

Lacombe, O., Laurent, P., 1992. Determination of principal stress magnitudes using calcite twins and rock mechanics data. Tectonophysics 202, 83–93.

Lacombe, O., 2001. Paleostress magnitudes associated with development of mountain belts: insights from tectonic analyses of calcite twins in the Taiwan Foothills. Tectonics 20, 834–849.

Lacombe, O., 2007. Comparison of paleostress magnitudes from calcite twins with contemporary stress magnitudes and frictional sliding criteria in the continental crust: mechanical implications. J. Struct. Geol. 29, 86–99.

Lacombe, O., 2010. Calcite twins, a tool for tectonic studies in thrust belts and stable orogenic forelands. Oil Gas Sci. Technol. – Revue d' IFP Energies Nouvelles 65 (6), 809–838.

Lacroix, B., Leclère, H., Buatier, M., Fabbri, O., 2013. Weakening processes in thrust faults: insights from the Monte Perdido thrust fault (southern Pyrenees, Spain). Geofluids 13, 56–65.

Lash, G.G., Engelder, T., 2007. Jointing within the outer arc of a forebulge at the onset of the Alleghanian orogeny. J. Struct. Geol. 29, 774–786.

Leclère, H., Daniel, G., Fabbri, O., Cappa, F., Thouvenot, F., 2013. Tracking fluid pressure buildup from focal mechanisms during the 2003-2004 Ubaye seismic swarm, France. J. Geophys. Res. 118, 1–16.

Love, J.D., Christiansen, A.C., 1985. Geologic map of Wyoming. U.S. Geol. Surv. 1, 500.000.

Marshak, Stephen, Karlstrom, K., Michael Timmons, J., 2000. Inversion of Proterozoic extensional faults: an explanation for the pattern of Laramide and Ancestral Rockies intracratonic deformation, United States. Geology 28, 735–738.

May, S.R., Gray, G.R., Summa, L.L., Stewart, N.R., Gehrels, G.E., Pecha, M.E., 2013. Detrital zircon geochronology from the bighorn basin, wyoming, USA: Implications for tectonostratigraphic evolution and paleogeography. GSA Bull. 125 (9/10), 1403–1422.

Michael, K., Bachu, S., 2001. Fluids and pressure distributions in the foreland-basin succession in the west-central part of the Alberta basin, Canada: evidence for permeability barriers and hydrocarbon generation and migration. AAPG Bull. 85 (7), 1231–1252.

Moore, J.C., Barrett, M., Thu, M.K., 2013. Fluid pressures and fluid flows from boreholes spanning the NanTroSEIZE transect through the Nankai Trough, SW Japan. Tectonophysics 600, 108–115.

Mourgues, R., Cobbold, P.R., 2003. Some tectonic consequences of fluid overpressures and seepage forces as demonstrated by sandbox modelling. Tectonophysics 376, 75–97.

Mourgues, R., Cobbold, P.R., 2006. Sandbox experiments on gravitational spreading and gliding in the presence of fluid overpressures. J. Struct. Geol. 28, 887–901.

Neely, T.G., Erslev, E.A., 2009. The interplay of fold mechanisms and basement weaknesses at the transition between Laramide basement-involved arches, north-central Wyoming, USA. J. Struct. Geol. 31, 1012–1027.
Nordgard Bolas, H., Hermanrud, C., Teige, G.M.G., 2004. Origin of overpressures in shales: constraints from basin modeling. AAPG Bull. 88 (2), 193–211.
Nysæther, E., 2006. Determination of Overpressures in Sandstones by Fluid-flow Modelling: The Haltenbanken Area, Norway, pp. 1–27.
Omar, G.I., Lutz, T.M., Giegengack, R., 1994. Apatite fission-track evidence for Laramide and post-Laramide uplift and anomalous thermal regime at the Beartooth overthrust, Montana-Wyoming. GSA Bull. 106, 74–85.
Pierce, W.G., Nelson, W.H., 1968. Geologic Map of the Pat O'Hara Mountain Quadrangle, Park County, Wyoming. In: U.S. Geological Survey, Geologic Quadrangle Map GQ-0755, vol. 1, p. 62,500.
Pierce, W.G., 1966. Geologic Map of the Cody Quadrangle, Park County, Wyoming. In: U.S. Geological Survey, Geologic Quadrangle Map GQ-542, vol. 1, p. 62,500.
Philipp, S.L., 2012. Fluid overpressure estimates from the aspect ratios of mineral veins. Tectonophysics 581, 35–47.
Pironon, J., Bourdet, J., 2008. Petroleum and aqueous inclusions from deeply buried reservoirs: experimental simulations and consequences for overpressure estimates. Geochim. Cosmochim. Acta 72, 4916–4928.
Raimbourg, H., Kimura, G., 2008. Non-lithostatic pressure in subduction zones. Earth Planet. Sci. Lett. 274, 414–422.
Rioux, R.L., 1994. Geologic Map of the Sheep Mountain – Little Sheep Mountain Area, vol. 1. U.S. Geological Survey, Big Horn County, Wyoming, p. 48,000.
Roberts, S.V., Burbank, D.W., 1993. Uplift and thermal history of the Teton Range (northwestern Wyoming) defined by apatite fission-track dating. EPSL 118, 295–309.
Roberts, L.N.R., Finn, T.M., Lewan, M.D., Kirschbaum, M.A., 2008. Burial History, Thermal Maturity, and Oil and Gas Generation History of Source Rocks in the Bighorn Basin, Wyoming and Montana. U.S. Geological Survey, p. 37. Scientific Investigations Report 2008-5037.
Roure, F., Andriessen, P., Callot, J.P., Faure, J.L., Ferket, H., Gonzales, E., Guilhaumou, N., Lacombe, O., Malandain, J., Sassi, W., Schneider, F., Swennen, R., Vilasi, N., 2010. The Use of Palaeo-thermo-barometers and Coupled Thermal, Fluid Flow and Pore-fluid Pressure Modelling for Hydrocarbon and Reservoir Prediction in Fold and Thrust Belts. In: Geological Society, London, Special Publications 348, pp. 87–114.
Roure, F., Swennen, R., Schneider, F., Faure, J.L., Ferket, H., Guilhaumou, N., Osadetz, K., Robion, P., Vandeginste, V., 2005. Incidence and importance of tectonics and natural fluid migration on reservoir evolution in foreland fold-and-thrust belts. Oil Gas Scie Technol 60, 67–106.
Savage, H.M., Shackleton, J.R., Cooke, M.L., Riedel, J.J., 2010. Insights into fold growth using fold-related joint patterns and mechanical stratigraphy. J. Struct. Geol. 32, 1466–1475.
Sibson, R.H., 1989. Earthquake faulting as a structural process. J Struct. Geol. 11 (1–2), 1–14. http://dx.doi.org/10.1016/0191-8141(89)90032-1.
Sibson, R.H., 2012. Reverse Fault Rupturing: Competition between Non-optimal and Optimal Fault Orientations. In: Geological Society, London, Special Publications 367, pp. 39–50.
Sibson, R.H., 2004. Controls on maximum fluid overpressure defining conditions for mesozonal mineralisation. J. Struct. Geol. 26, 1127–1136.
Sibson, R.H., 2013. Stress switching in subduction forearcs: implications for overpressure containment and strength cycling on megathrusts. Tectonophysics 600, 142–152.
Siddoway, C., Anderson, M., Erslev, Eric, 2011. Formation of basement-involved foreland arches: integrated structural and seismological research in the Bighorn Mountains, Wyoming. In: Varga, R.J., Frey, H., Morgan, C., Kadyk, D. (Eds.), 24th Annual Keck Symposium, pp. 1–8.
Smith, A.P., Fischer, M.P., Evans, M.A., 2013. On the homogeneity of fluids forming bedding-parallel veins. Geofluid. http://dx.doi.org/10.1111/gfl.12040.
Stanton, H.I., Erslev, E.A., 2004. Sheep Mountain Anticline: Backlimb Tightening and Sequential Deformation in the Bighorn Basin, Wyoming. In: 53rd Guidebook. Wyoming Geological Association, Casper, pp. 75–87.
Stearns, D.W., 1971. Faulting and forced folding in the Rocky Mountains foreland. In: Matthews, V. (Ed.), Laramide folding associated with basement block faulting in the western United States, vol. 151Geological Society of America Memoir, pp. 1–37.
Stone, D.S., 1987. Northeast-southwest structural transect: Rocky mountain foreland, wyoming (abs.). AAPG Bull. 71, 1015, 1:24.000.
Suppe, J., Chou, G.T., Hook, S.C., 1991. Rates of folding and faulting determined from growth strata. In: McClay, K.R. (Ed.), Thrust Tectonics. Chapman & Hall, London, pp. 105–121.
Thomas, L.E., 1965. Sedimentation and structural development of Big Horn Basin. AAPG Bull. 49 (11), 1867–1877.
Van Geet, M., Swennen, R., Durmishi, C., Roure, F., Muchez, P.H., 2002. Paragenesis of Cretaceous to Eocene carbonate reservoirs in the Ionian fold and thrust belt (Albania): relation between tectonism and fluid flow. Sedimentology 49, 697–718.
Van Ruth, P., Hillis, R., Tingate, P., 2004. The origin of overpressure in the Carnarvon Basin, Western Australia: implications for pore pressure prediction. Pet. Geosci. 10, 247–257.
Varga, R.J., 1993. Rocky Mountain foreland uplifts:Products of rotating stress field or strain partitioning? Geology 21, 1115–1118.
Weil, A.B., Yonkee, W.A., 2012. Layer-parallel shortening across the Sevier fold-thrust belt and Laramide foreland of Wyoming: spatial and temporal evolution of a complex geodynamic system. Earth Planet. Sci. Lett. 357-358, 405–420.
Yassir, N.A., Bell, J.S., March 1996. Abnormally high pressures and associated porosities and stress regimes in sedimentary basins. SPE Format. Evaluat., 5–10.
Yu, Z., Lerche, I., 1996. Modelling abnormal pressure development in sandstone/shale basins. Marine Pet. Geol. 13, 179–193.
Zoback, M.D., Townend, J., 2001. Implications of hydrostatic pore pressures and high crustal strength for the deformation of intraplate lithosphere. Tectonophysics 336, 19–30.